

# Irradiated Pulsar Planets and Companions as 511 keV Positron Annihilation Line Sources

Zachary Metzler<sup>1,2,3</sup> and Zorawar Wadiasingh<sup>1,2,3</sup>

<sup>1</sup>*University of Maryland, College Park*

<sup>2</sup>*NASA Goddard Space Flight Center*

<sup>3</sup>*Center for Research and Exploration in Space Science & Technology II*

(Dated: March 14, 2025)

## Abstract

Millisecond pulsars (MSPs) are prolific GeV  $\gamma$ -ray emitters, and nearly 80% of Fermi-LAT MSPs reside in compact binaries. We demonstrate that the companions in these compact MSPs binaries are also 511 keV annihilation line emitters using MEGALIB simulations (a high energy radiation transport software built with Geant4) to compute the particle showers and resulting backscplash emission from the pulsar irradiation. The 511 keV signal exhibits strong flux modulation and red/blueshifts associated with a binary orbit, enabling powerful coherent searches. Measuring the 511 keV emission would enable direct  $\gamma$ -ray characterization of unusual pulsar exoplanets and companions, and allow one to identify the unambiguous presence of active pulsars whose beams do not intercept Earth. Intriguingly, the 511 keV flux is brightest for ultra-compact systems against which pulsar surveys are systematically biased. These ultra-compact systems are also possibly prime LISA galactic sources. This necessitates future joint LISA-MeV  $\gamma$ -ray techniques to characterize MSP binaries. These MSP binaries may also contribute to the puzzling source of the excess 511 keV photons near the galactic bulge and center.

*Introduction* The sources of 511 keV photons from the galaxy, measured with INTEGRAL SPI, are unresolved [1–5]. Similarly, the origin of the *Fermi* Large Area Telescope (LAT) [6] galactic center GeV  $\gamma$ -ray excess is a mystery [7]. Many sources have been proposed to contribute to these excesses, including dark matter annihilation [7–10], point-like X-ray binary jets [11], or an unresolved population of pulsars near the galactic center [12]. COSI, an upcoming MeV  $\gamma$ -ray explorer that will launch in 2027 [13], aims to resolve the 511 keV excess, and several MeV  $\gamma$ -ray observatory concepts of varying capability, including AMEGO [14], AMEGO-X [15], GECCO [16], GRAMS [17], GammaTPC [18], and APT [19], could also settle the 511 keV excess question.

Millisecond pulsars (MSPs) canonically form by accreting material from a companion star that increases the angular velocity of a neutron star (NS) [20–23]. Most MSPs are excellent GeV photon  $\gamma$ -ray emitters [24] from their outer magnetosphere and equatorial current sheets, with produced  $\gamma$ -rays preferentially collimated in equatorial latitudes perpendicular to MSP’s spin axis [e.g., 25–35]. As a consequence of the spin-up formation process, MSP’s spin and orbital momentum vectors are close to alignment. Thus, the companions of MSPs generally experience significant pulsed GeV  $\gamma$ -ray irradiation fluxes.

Nearly 80% of detected  $\gamma$ -ray MSPs have binary companions [24], the majority of which are He white dwarfs (WDs), but can also be Carbon-Oxygen (CO) WDs, brown dwarfs (BD), main sequence-like stars (MS) or ultralight (UL) companions with mass  $\ll 0.1M_{\odot}$  and unknown composition [36, 37]. Two interesting classes of binary pulsar systems are black widow (BW) and redback (RB) pulsars [38, 39]. These compact binaries typically have orbital periods  $< 2$  days and are differentiated by the companion masses,  $\ll 0.1M_{\odot}$  and  $> 0.1M_{\odot}$  for BWs

and RBs, respectively. Owing to strong irradiation for many Myr, BW and RB systems have poorly-understood atmospheric structures and composition [40–44]. Their atmospheres are perhaps ablated of lighter elements with possible lithium enrichment from bombardment and spallation by relativistic species or  $\gamma$ -rays [45–47].

UL companions, which might also exist in triples/multiples [48, 49], may form in a high metallicity accretion disk over  $> 1$  Gyr [50] or via exchange interactions and capture in a cluster [51], as they may not survive the supernova which produced the NS. Another possibility for UL companion formation, and particularly for BW systems, is by accretion of an ultra-compact X-ray binary companion’s outer layers onto the NS [52]. A severe bias exists against detection of pulsars in ultra-compact binaries (UCBs), owing to Doppler smearing of pulses [53–55] or infeasible computational cost [56–58]. Studies, accounting for this bias, suggest there may be  $\sim 7000$  MSP-WD UCBs with  $P_{\text{orb}} \lesssim 15$  min in the galaxy [55]. X-ray studies point to even higher numbers, perhaps  $\sim 10^5$  UCBs in the bulge [59]. UCBs also emit gravitational waves (GWs) with frequency  $f_{\text{GW}} > 10^{-5}$  Hz, and numerous studies estimate that the Laser Interferometer Space Antenna (LISA) will detect  $\sim 100$  NS-WD UCBs [60–67], most of whose pulsars will not be beamed toward Earth.

In this study, we consider for the first time the bombardment of a range of companion types by the pulsar’s primary high energy  $\gamma$ -rays and the resulting shower of secondary lower energy  $\gamma$ -rays and  $e^{-}e^{+}$  pairs, as depicted in Figure 1. Prior studies have considered companion heating through bombardment of  $e^{-}e^{+}$  pairs [68], or bombardment of a companion by TeV protons [69], but neither conceived of the possibility of 511 keV backscplash emission. We model 12 representative systems with Cosima [70], which is a Geant4-based [71] Monte

Carlo simulator, injecting high energy  $\gamma$ -rays with a fiducial luminosity  $L_{\text{MSP}} = 10^{34}$  ergs/s and a representative spectrum for MSPs in the 3rd *Fermi*-LAT Pulsar Catalog [24]. We present the resulting spectra and their geometric, orbital and composition dependencies (see the Appendix for details). Finally, we examine the predicted signals from known MSP binary systems.

*Unimportance of Plasma Effects* **Geant4**, and by extension **Cosima**, assumes non-ionized material rather than a plasma for its test particle shower simulation. The stopping power of errant ionized gas or coronae around companions in pulsars to  $\gamma$ -rays is generally negligible. The primary  $\gamma$ -rays and associated particle energies are also well above where most atomic transitions are significant. Thus, to a good approximation, scattering of photons by electrons in the simulation behaves as that by free electrons. Coulomb losses for created pairs are dominant in the incipient shower<sup>1</sup>. Collective effects here may be neglected in the limit that the Debye length,  $\lambda_D = \sqrt{\epsilon_0 k_B T_e / (n_e q_e^2)}$ , is shorter than the mean free path ( $\epsilon_0$  is the permittivity of free space,  $k_B$  the Boltzmann constant,  $T_e$  the electron temperature,  $n_e$  the electron number density, and  $q_e$  the electron charge). Charged particle energies are generally well above typical background plasma thermal energies,  $kT_e \ll 1$  keV. As realized temperatures are not relativistic, thermal line broadening will also be minimal. The mean free path is approximated by the continuous slowing down approximation (CSDA) range,  $R_{\text{CSDA}}$  used by NIST ESTAR [72] as  $\lambda_{\text{MFP}} = R_{\text{CSDA}} / \rho = R_{\text{CSDA}} / (m_p A n_e)$ , where  $\rho = m_p A n_e$  is the material density,  $m_p$  is the proton mass and  $A$  is the atomic mass number of the material,

$$\frac{\lambda_D}{\lambda_{\text{MFP}}} = \frac{\sqrt{\epsilon_0 k_B T_e n_e m_p A}}{q_e R_{\text{CSDA}}} < 1. \quad (1)$$

The condition Equation 1 is generally satisfied for BD, MS, and WD models, including their ionized atmospheres. The planets ought not be appreciably ionized, and their atmospheres should be both lower density and lower temperature than the extremes of the stellar companion models. For the BD and MS models, the highest product of density and temperature is in the core of the 0.1  $M_\odot$  MS star at 450 g/cm<sup>3</sup> and  $2 \times 10^7$  K. The C WD is assumed to have 10<sup>6</sup> K surface temperature, and the inner structure is negligible due to the high density and limited penetration depth. The smallest  $R_{\text{CSDA}}$  are thus realized for low energy electron/positrons that could be produced in the shower of the primary high energy  $\gamma$ -rays.

Magnetic fields are neglected; however it is likely magnetic bremsstrahlung would actually enhance the escape

of the 511 keV line by reducing shower depth.

*Primary Irradiation Channels* The 511 keV line luminosity may be sourced by multiple channels: (i) direct irradiation of the companion's surface by the pulsar's GeV  $\gamma$ -rays (ii) relativistic  $e^-e^+$  pairs produced at polar cap cascades [73] and advected into the pulsar wind which might impact the companion (iii) ultra-relativistic 10-100 TeV  $e^-e^+$  pairs [74, 75], which produce the pulsar's GeV emission via curvature radiation, accelerated proximate to the pulsar current sheet that are essentially radial in direction and impact the companion (iv)  $>$ TeV ions extracted from the neutron star crust, potentially reaching a few percent of the spin-down luminosity of the MSP [76] (v) intrabinary shock re-acceleration of polar cap pairs to TeV energies, producing synchrotron and inverse Compton  $\gamma$ -rays [77–79] which irradiate the companion. Channels (i)-(iv) occur in every  $\gamma$ -ray emitting pulsar in a binary, while channel (v)'s efficacy is largely limited to the spider binaries, the BWs and RBs where shock emission is significant. Thus the total 511 keV line luminosity is

$$L_{511} = L_{511,i} + L_{511,ii} + L_{511,iii} + L_{511,iv} + L_{511,v}. \quad (2)$$

The maximum 511 keV backplash emission is  $L_{511} < \dot{E} \Delta\Omega$ , where  $\Delta\Omega$  is the solid angle of the companion from the MSP's perspective. Below we appraise the first of the five possible contributions to  $L_{511}$ , as that contribution's primaries are observationally most well understood and least affected by magnetic fields, and our results may be conservative estimates by considering only the one irradiation channel. The other contributions are briefly addressed in the supplemental material.

*Secondary Emission Simulations* We ran simulations of 12 spherical companion models: 5 planets (He, C, S, Si, and Fe), 2 WDs (He, C), 1 BD, and 4 MS stars (0.03, 0.1, 0.3, and 0.9  $M_\odot$ ). Each primary  $\gamma$ -ray that interacts with the companion produces a shower of daughter  $\gamma$ -rays, electrons, and positrons that are all tracked until absorption or escape in 3D. The most prominent interactions that yield 511 keV photons for a representative C WD model are shown in Figure 2. Most 511 keV production stems from the 1st, 2nd, or 3rd generation of pair production and bremsstrahlung, terminating with  $e^-e^+$  annihilation. This requires the dominance of continuous Coulomb (not depicted) and bremsstrahlung losses of charges and absence of scattering interactions by parent photons of the 511 keV  $\gamma$ -rays. The full range of pathways is detailed in the Appendix (Fig. 8).

We define the 511 keV production efficiency,  $\epsilon$ , in Equation 3, where  $\dot{N}_{511}$  is the total luminosity of 511 keV photons escaping the system in units of photons/s, and  $\int_{E_{\text{min}}}^{E_{\text{max}}} \frac{dN}{dE} dE = 1$ . Table I lists  $\epsilon$  for each model. Equation 3 also shows that, keeping the companion and MSP properties constant,  $\dot{N}_{511}$  is linear with  $\Delta\Omega$ , so there will be more backplash 511 keV emission from a compact binary or a binary with a larger companion.

<sup>1</sup> The **Cosima** simulations of tagged "ionization" losses in a nonionized material are compatible with the Coulomb stopping power of a cold electron-ion plasma.

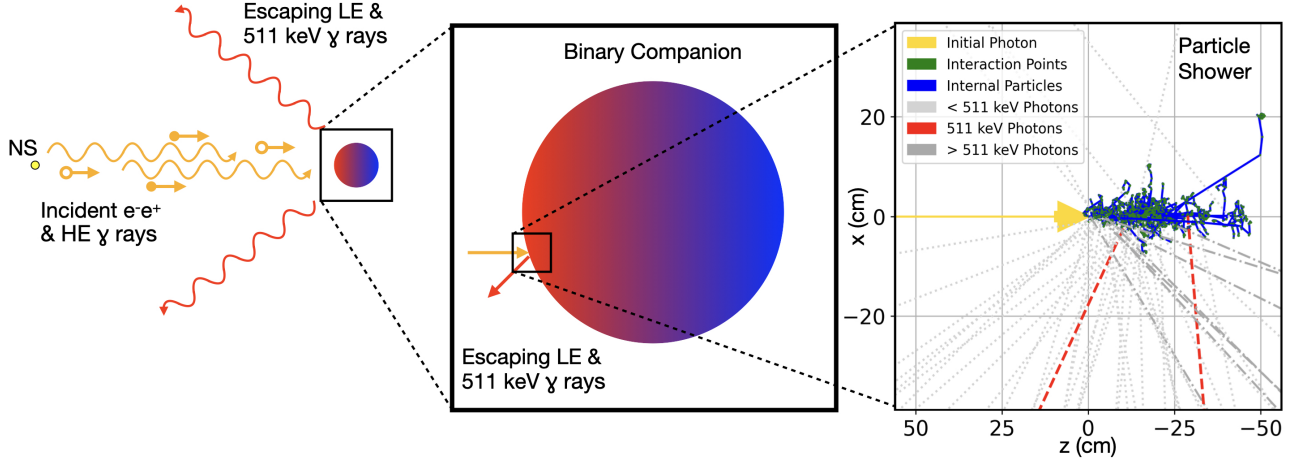


FIG. 1. Schematic of a MSP irradiating its companion with high energy  $\gamma$ -rays and charged particles. These primary particles bombard the surface of the companion, which are reprocessed into low energy backplash  $\gamma$ -rays, low energy  $e^-e^+$  pairs, and 511 keV line emission that escape from the system. In the rightmost panel,  $x = 0$  corresponds to incident  $\gamma$ -ray's path, and  $z = 0$  corresponds to the surface of the companion along that path.

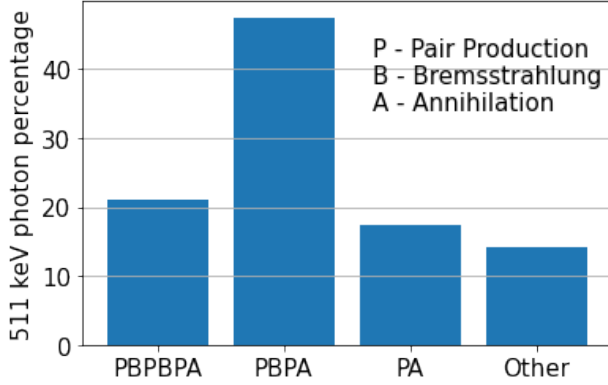


FIG. 2. Histogram of the most dominant pathways for escaped 511 keV photons for a representative C WD. These represent multiple generations of  $e^-e^+$  pair production and  $\gamma$ -ray production through bremsstrahlung that concludes with  $e^-e^+$  annihilation, creating an escaping 511 keV  $\gamma$ -ray.

$$\epsilon = \dot{N}_{511} \times \frac{\int_{E_{\min}}^{E_{\max}} \frac{dN}{dE} E dE}{L_{\text{MSP}}} \times \frac{4\pi}{\Delta\Omega} \quad (3)$$

The annihilation line  $\gamma$ -ray emission is not isotropic, so in Equation 4 we define a differential  $\gamma$ -ray emissivity,  $\dot{n}_{511}(\phi, i)$  (units of photons/s/sr), escaping at an azimuthal angle in the orbital plane,  $\phi$ , and inclination angle,  $i$ .  $\phi = 0$  is defined as directly towards the MSP, and  $i = 0$  is orthogonal to the orbital plane. Table I lists  $\dot{N}_{511}$  and the maximum of  $\dot{n}_{511}(\phi, i = \pi/2)$  for each model, assuming a distance of 100 pc from Earth.

$$\dot{N}_{511} = \iint d\phi di \sin(i) \dot{n}_{511}(\phi, i) \quad (4)$$

Model	$a_{10}$	$P_{\text{orb}}$	$R_{\text{comp}}$	$\epsilon$ (%)	Peak $\dot{n}_{511}$	$\dot{N}_{511}$
Units	—	$10^4 \text{s}$	$10^8 \text{cm}$	%	$\text{ph}/\text{cm}^2/\text{s}$	$\text{ph}/\text{s}$
He planet	8.8	1.1	6	2	$10^{-12.0}$	$10^{29.8}$
C planet	8.8	1.1	6	10	$10^{-11.4}$	$10^{30.5}$
Si planet	8.8	1.1	6	42	$10^{-10.8}$	$10^{31.2}$
S planet	8.8	1.1	6	54	$10^{-10.6}$	$10^{31.3}$
Fe planet	8.8	1.1	6	126	$10^{-10.3}$	$10^{31.6}$
He WD	9.7	1.2	200	2	$10^{-9.1}$	$10^{32.8}$
C WD	2.3	0.12	7	10	$10^{-10.1}$	$10^{31.8}$
$0.01 M_{\odot}$ BD	8.0	0.94	69	1	$10^{-10.0}$	$10^{31.8}$
$0.03 M_{\odot}$ MS	4.9	0.45	60	1	$10^{-9.7}$	$10^{32.2}$
$0.1 M_{\odot}$ MS	4.7	0.41	83	1	$10^{-9.5}$	$10^{32.4}$
$0.3 M_{\odot}$ MS	8.2	0.90	200	1	$10^{-9.2}$	$10^{32.8}$
$0.9 M_{\odot}$ MS	17	2.4	550	1	$10^{-8.9}$	$10^{33.0}$

TABLE I. For each companion model, the number of photons between 505 and 515 keV per interacting primary  $\gamma$ -ray is reported. The 511 line flux assumes a pulsar luminosity of  $10^{34}$  erg/s, and a distance of 100 pc from Earth.

The He WD and massive star systems have the brightest 511 keV line at  $10^{-8.9}$  and  $10^{-9.1}$   $\text{ph}/\text{cm}^2/\text{s}$  at 100 pc. A spectrum for the secondary emission from the He WD system is shown alongside the initial MSP spectrum in Figure 3, demonstrating that the backplash emission rises above the MSP's primary continuum emission (which are generally not beamed toward the observer in similar directions) by a factor of  $\sim 10$  at 511 keV. For fainter models, the line may not rise above the pulsar emission, complicating searches for the emission from these systems, and indicating that searches would be more sensitive to binary MSP systems with harder primary  $\gamma$ -ray spectra than our assumption or whose pulsar emission is not beamed toward Earth. Figure 4 shows

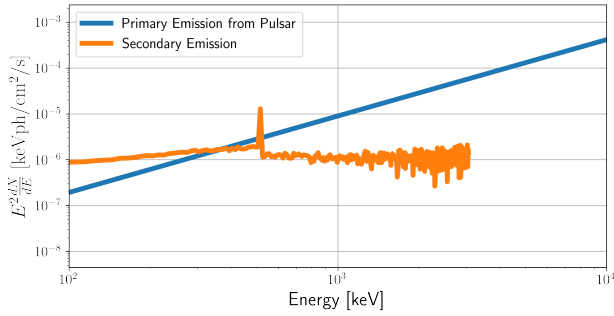


FIG. 3. Primary incident (blue) and secondary (orange) emission for an irradiated He WD. The MSP spectrum is defined by Equation A.7 with  $x = E/E_0$ ,  $E_0 = 2$  GeV,  $\Gamma = 1$ ,  $d = 0.6$ ,  $b = 0.9$ , and  $E$  is the incident  $\gamma$ -ray energy. This system is assumed to be 100 pc from Earth, and the pulsar luminosity is  $L_{\text{MSP}} = 10^{34}$  ergs/s. The normalization for this spectrum is averaged over all emission directions, and the instantaneous spectrum can vary by viewing angle.

the secondary emission spectrum for the same system as a function of orbit phase. An orbital Doppler shift modulates the line by  $\lesssim 1$  keV, neglecting the finite size of the companion. Figure 5 shows  $\dot{n}(\phi, i)$  for the C WD model, where the centers of the figure corresponds to the inferior conjunction of the MSP. This demonstrates how the inclination angle might be constrained by observing the variability of the secondary  $\gamma$ -ray emission throughout the orbit.

*Observability of Known Systems* We now consider binary MSPs with circular orbits in the ATNF Pulsar Catalogue [80]. The systems are divided based on the ‘BINCOMP’ column in the ATNF Pulsar Catalogue. Systems defined as ‘He’ or ‘HeT’ use the He WD model, those defined as ‘CO’ use the C WD model, and those defined as ‘MS’ happened to be RB systems with  $P_{\text{orb}} < 2$  days and used the MS model with the closest mass. The systems defined as ‘UL’ or ‘ULT’ were further divided into BWs, if  $P_{\text{orb}} < 2$  days, or UL otherwise. We assume  $1.7 M_{\odot}$  NSs and that the stellar companions’ radii are the value listed in Table I. The BW and UL systems are treated differently due to their unknown compositions. We make three different assumptions for the BW and UL companions: a) the companion density is  $10 \text{ g/cm}^3$ , b) the companion density is  $30 \text{ g/cm}^3$ , and c) the companion radius is  $6 \times 10^8 \text{ cm}$ . For reference, the companion orbiting J1719–1438 has a minimum density of  $22 \text{ g/cm}^3$  [a ‘diamond’ planet, 52]. In any case where the Roche lobe radius is less than the assumed radius, we use the Roche lobe radius instead. We assume  $L_{\text{MSP}} = 0.2\dot{E}$  and the same primary  $\gamma$ -ray spectrum as in the previous section. The systems and their parameters are listed in the supplemental material.

The maximum of  $\dot{n}_{511}(\phi, i = \pi/2)$  for these systems are summarized in Figure 6. The brightest source is J1720–0533 (hereafter J1720), but the distance to J1720 may

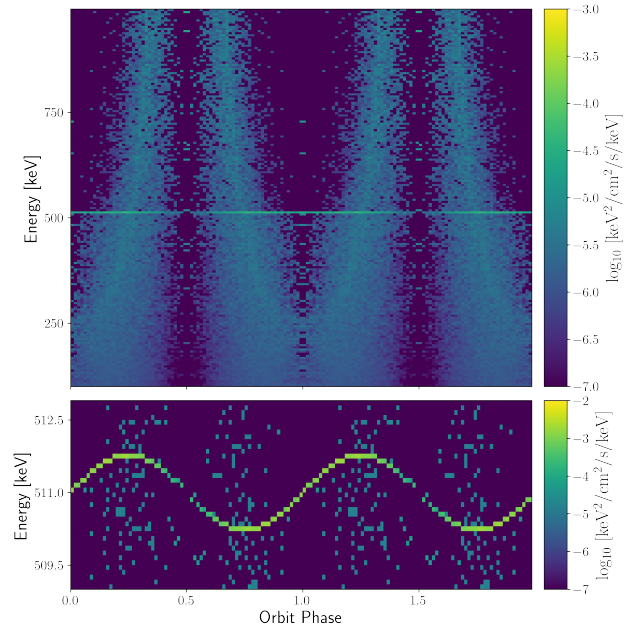


FIG. 4. The backsplash spectrum, and radial Doppler shifts (for zero systemic/peculiar velocity), for a He WD-MSP binary 100 pc from Earth viewed edge-on over the course of an orbit. Orbit phase = 0 corresponds to the inferior conjunction of the MSP. The 511 keV line shifts by  $\sim 1$  keV, which could substantially increase the sensitivity of coherent searches for the line emission if the Doppler shift can be resolved.

be underestimated by up to a factor of 5 [81]. COSI has a planned line sensitivity of  $1.2 \times 10^{-5}$  ph/cm<sup>2</sup>/s [13]. Coherent searches for a periodic signals gain a sensitivity improvement of  $\sqrt{T_{\text{obs}}/P_{\text{orb}}} \sim 30 - 300$  with  $P_{\text{orb}} = 10^3 - 10^4$  s and  $T_{\text{obs}} = 10^7 - 10^8$  s. Nevertheless, J1720 would not be individually detectable with COSI, and observations would likely rely on stacking analyses of many systems similar to J1720. Given the beaming geometry of MSPs [82, 83], the true source density of systems similar to J1720 (whose pulsars are not beamed toward Earth) ought to be a factor  $\mathcal{O}(10)$  or more higher than what has been observed to date.

In contrast with the previous section, the MSP-He WD population is considerably less bright in 511 keV line emission than the BW or RB populations. The reduction is due to the observed MSP-He WD binary systems being considerably further apart than the initial model, reducing  $\Delta\Omega$ , which scales as  $a_{10}^{-2}$  for small  $\Delta\Omega$ . The observational bias against UCBs in pulsar surveys is even more so for systems with heavier companions that exacerbate Doppler smearing [55]. Rescaling our He WD model such that  $P_{\text{orb}} \sim 25 \text{ min}^2$ , which is just before the system becomes an UCXB according to [62], yields

<sup>2</sup> This new geometry no longer follows the far-field source approximation used in the simulations, so the modulation with the orbit

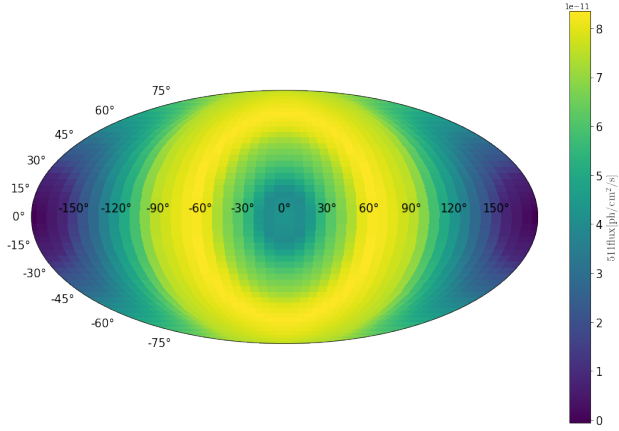


FIG. 5.  $\dot{n}_{511}(\phi, i)$  for the C WD model 100 pc from Earth. The center of the “eye” is the inferior conjunction of the MSP. The relative difference in flux of the center of the “eye” and bright ring correlates with the atomic number,  $Z$ , of the companion. In this way, an edge-on view of this system could constrain the companion composition. This effect is discussed in more detail in the Supplemental Material.

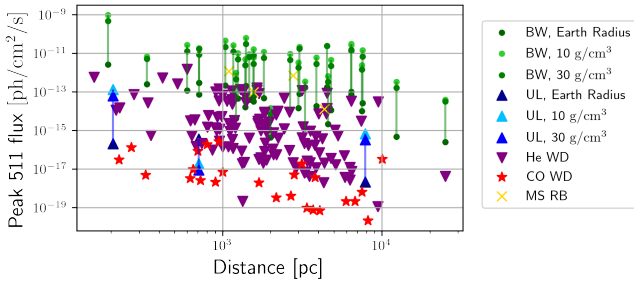


FIG. 6. The estimated flux for the MSP binary system in the ATNF Pulsar Catalogue. The BW and UL systems are modeled using three size assumptions a) the companion radius is  $6 \times 10^8$  cm, b) the companion density is  $10 \text{ g/cm}^3$ , and c) the companion density is  $30 \text{ g/cm}^3$ . In any case where the Roche lobe radius is less than the assumed radius, we use the Roche lobe radius instead. The BW systems are the most promising known candidates for observation.

a peak  $\dot{n}_{511}$  of  $5 \times 10^{-9} \text{ ph/cm}^2/\text{s}$  at 100 pc, and gains a coherent search sensitivity boost  $\sim 80$  for COSI. An even larger sensitivity boost by an additional factor of  $\sim \sqrt{T_{\text{obs}}/P_{\text{orb}}}$  may be afforded with energy-dependent coherent searches exploiting the larger Doppler modulation of UCBs, provided a sufficient amount of photons are collected. The coherent search prospects for COSI and other, more sensitive, MeV observatory concepts require dedicated simulations beyond the scope of this work, and the bias against UCBs in pulsar surveys

will change; this departure likely makes the “eye” shape from Figure 5 smaller and even brighter, potentially benefiting detectability.

necessitates alternative searches for these systems, not subject to the above constraints, such as with gravitational waves (GWs).

*Potential LISA Sources* Compact ( $P_{\text{orb}} \lesssim 2$  days) MSP binary systems are GW emitters with frequencies,  $f_{\text{GW}} > 10^{-5} \text{ Hz}$ . Following the procedure from Robson et al [84] for binary systems, one can calculate the location, inclination, and polarization averaged strain spectral density for a nearly monochromatic binary system,

$$h_{\text{GB}}(f_{\text{GW}}) = \sqrt{\frac{2T_{\text{obs}}\dot{f}_{\text{GW}}}{3} \frac{(GM_c/c^3)^{5/6}}{\pi^{2/3}f_{\text{GW}}^7(D/c)}} \quad (5)$$

where  $T_{\text{obs}}$  is the mission lifetime,  $M_c = (M_{\text{NS}}M_{\text{comp}})^{3/5}(M_{\text{NS}} + M_{\text{comp}})^{-1/5}$  is the chirp mass,  $D$  is the distance of the binary, and  $f_{\text{GW}} = 2/P_{\text{orb}}$  is the GW frequency.  $\dot{f}_{\text{GW}}$  is given in Eq. 6 below for the case when GWs dominate the decay of the orbit, but non-gravitation effects such as companion mass loss and magnetic torques may alter the evolution.

$$\dot{f}_{\text{GW}} = \frac{96}{5}\pi^{8/3}(GM_c/c^3)^{5/3}f_{\text{GW}}^{11/3} \quad (6)$$

As an example, we consider J1720, a BW system with a  $0.034M_{\odot}$  companion, 3.2 hr orbit, and is the brightest system from Figure 6. Assuming GW-driven orbit decay, J1720 has a  $h_{\text{GB}} = 9.7 \times 10^{-19} \text{ Hz}^{-1/2}$ , which falls near the LISA design sensitivity at  $f_{\text{GW}} = 0.18 \text{ mHz}$  for a 4 year mission. It is possible that the companion mass is underestimated for J1720 as the orbital inclination angle is poorly constrained, which would lead to an increase in GW strain amplitude.

For the models in Table I, we focus on a compact binary with a He WD companion. Assuming GW-driven orbit decay, such a system would have  $f_{\text{GW}} = 0.17 \text{ mHz}$  and  $h_{\text{GB}} = 8.4 \times 10^{-18} \text{ Hz}^{-1/2}$ , which yields an SNR  $\sim 1$  at 100 pc. Given the strong bias against pulsar UCBs, only a few similar compact binaries have been observed in a pulsar state, but LISA is sensitive to nearly the whole galaxy for those in UCXB states [62], and LISA searches do not experience the same degradation due to Doppler smearing. Rescaling our He WD model to just before the system becomes an UCXB according to [62] yields a LISA SNR  $\sim 200$  at 100 pc. Conveniently, the brightest 511 keV sources are also the loudest LISA sources, so such a system could be observable with a future MeV observatory [e.g., 18]. Discovery of UCBs with LISA would define an ensemble of high-value systems for analyses with COSI and other observatories that would be unavailable with radio pulsar surveys due to Doppler smearing. Likewise, optical surveys for low mass planets or companions of unseen pulsars in the Galactic plane are strongly constrained by sensitivity, crowding and extinction.

*Conclusion* We introduce a new class of astrophysical 511 keV sources, (ultra-)compact binary MSP systems. We find compact He WD and massive MS binaries

are the brightest companion types with  $\dot{N}_{511}$  up to  $10^{33}$  photons/s when the companion is the size of its Roche lobe. Given strong observational biases against pulsar UCBs, there likely exists a vast unobserved population of UCB systems with even brighter 511 keV lines. Such systems may be observable by both LISA and future soft  $\gamma$ -ray instruments, providing a method to identify active pulsars whose pulsed emission is not beamed toward Earth. Among the currently observed binaries, BWs are the brightest systems. In particular, the potentially high-Z BW system, J1720, may have annihilation line emission peaking  $\sim 10^{-9}$  ph/cm<sup>2</sup>/s. Observations of the 511 keV line and its modulation constrain the orbital parameters, companion composition, and evolutionary history of the binary, opening the possibility for  $\gamma$ -ray exoplanet characterization.

A large number ( $\gtrsim 10^5$ ) of MSPs in UCBs [as proposed by some X-ray studies, e.g., 11, 59] would be required to significantly contribute to the 511 keV excess in our scenario. Other sources of primary radiation for these systems have been neglected in this study, so this study represents a conservative estimate of the line emission flux. COSI observations would likely rely on joint observations with either radio pulsar surveys or LISA to define targets for stacking analyses, motivating a study of dedicated  $\gamma$ -ray observatory concepts to search for this emission. Some remaining open questions are the prominence of hadronic interactions and nuclear lines due to ion bombardment (which planned instruments may be even more sensitive to than the 511 keV line), the contribution of MSP binaries to the unresolved galactic diffuse emission, the enhanced 511 keV line emission due to bombardment by relativistic species and shock emission in some binaries. Finally, such detailed studies open the possibility in the future to probe the unknown content of relativistic particle species accelerated by pulsars, and assess their relevance to cosmic rays.

*Acknowledgments* We acknowledge helpful discussions with Aimee Hungerford, Peter Shawhan, and Regina Caputo. The material is based upon work supported by NASA under award number 80GSFC24M0006. This work has made use of the NASA Astrophysics Data System.

## Appendix

*Companion Size and Composition Specification* Due to the uncertain composition of the planets in pulsar binary systems, we consider 5 different compositions consisting of He, C, S, Si, and Fe. We assume homogeneous spheres of density  $10 \text{ g cm}^{-3}$  and radius  $6 \times 10^8 \text{ cm}$ , which is approximately Earth’s mass and radius. In essence, these models physically represent planets with a dense core and variable crust compositions, but considering a homogeneous sphere is simpler and should not affect the results due to the limited penetration depth into the crust of a C planet. Figure 1 shows an example photon shower for the C planet, which penetrates  $\sim 50 \text{ cm}$  below the surface. The penetration depth varies greatly with density, with the planets having their first photon interaction  $\lesssim 15 \text{ cm}$  below the surface, compared to  $\lesssim 10^8 \text{ cm}$  for the  $0.3M_\odot$  MS model, discussed below. We also neglect atmospheres around the planets, because of stripping of atmospheres from pulsar irradiation leading to negligible interaction probability of gamma rays  $> 500 \text{ keV}$  around possible tenuous hot coronae.

The semimajor axis,  $a_{10}$ , is assumed to be the closest orbit without Roche lobe overflow. For a circular orbit  $a_{10}$  is equal to the orbit radius. We use the approximation for Roche lobe radius of [85], and we assume NS of mass  $1.7M_\odot$ .  $a_{10}$  for each model is listed in Table I.

We consider both C and He WD models. We initially considered a uniform sphere with density  $10^6 \text{ g cm}^{-3}$  and radius  $7 \times 10^8 \text{ cm}$  for the C WD, but we suspected that there were truncation errors during the simulation due to the small radiation lengths. Therefore, for the C WD we use the same simulation as the carbon planet and scale the results according to the new mass, companion radius, and  $a_{10}$ . Assuming C WD fills its Roche lobe led to an orbital period of 39 s, which would be very close to merger, so to have a realistic longer-lived system, we increased  $a_{10}$  by a factor of 10. For the He WD, we use the same simulation as the He planet, but we scale the results to a solid angle corresponding to a radius of  $2 \times 10^{10} \text{ cm}$  and recalculate  $a_{10}$ .

In addition to the homogeneous sphere models, we consider a BD star with mass  $0.01 M_\odot$  and four MS stars with masses of 0.03, 0.1, 0.3, and  $0.9 M_\odot$ . Their compositions and densities were determined using the Modules for Experiments in Stellar Astrophysics (MESA) software package [86–91]. The MESA EOS is a blend of the OPAL [92], SCVH [93], FreeEOS [94], HELM [95], PC [96], and Skye [97] EOSes. Radiative opacities are primarily from OPAL [98, 99], with low-temperature data from Ferguson et al. [100] and the high-temperature, Compton-scattering dominated regime by Poutanen [101]. Electron conduction opacities are from Cassisi et al. [102] and Blouin et al. [103]. Nuclear reaction rates are from JINA REACLIB [104], NACRE [105] and additional tab-

ulated weak reaction rates Fuller et al. [106], Oda et al. [107], Langanke and Martínez-Pinedo [108]. Screening is included via the prescription of Chugunov et al. [109]. Thermal neutrino loss rates are from Itoh et al. [110]. The model evolution of the 0.1, 0.3 and  $0.9 M_\odot$  MS stars is near ZAMS, while the 0.01 and  $0.03 M_\odot$  star models were evolved for 2 Gyr before stopping. The initial conditions for the four MS stars are the standard pre main sequence model from MESA, and the initial conditions for the BD star is the standard when creating a generic initial model with the metallicity described in [111]. Figure 7 shows the density profiles for the BD and MS stars.

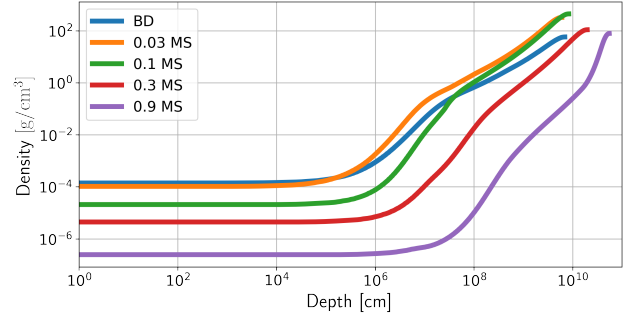


FIG. 7. Density profiles of BD and MS stars calculated with MESA.

*Monte Carlo Simulations with Cosima* A Monte Carlo simulation for each companion is performed with Cosima, the Cosmic Simulator of MEGALIB, the Medium Energy Gamma-ray Astronomy library [70], which utilizes the GEANT4 simulation toolkit [112] for particle transport. The source for the simulation is assumed to be a far-field point source irradiating a spherical geometry with gamma rays. The spectrum for the gamma rays is a power law with exponential cutoff as in Equation A.7, where  $x = E/E_0$ ,  $E_0 = 2 \text{ GeV}$ ,  $\Gamma = 1$ ,  $d = 0.6$ ,  $b = 0.9$ , and  $E$  is the incident gamma ray energy.

$$\frac{dN}{dE} \propto x^{(-\Gamma+d/b)} \times e^{(d/b^2+(1-x^b))} \quad (\text{A.7})$$

These values are meant to be representative of the gamma ray spectra in Table 14 of the 3rd Fermi Large Area Telescope Pulsar Catalog (3PC) [24]. We assume  $L_{\text{MSP}} = 10^{34} \text{ erg/s}$  as a representative value, which may be readily scaled up or down.

*Time Scales* MSPs have pulsed GeV gamma ray emission with  $P_{\text{MSP}} < 30 \text{ ms}$ , but the pulsed emission is neglected in the simulations due to smeared arrival times at the companions. At minimum, photon arrival and escape times for one of the planets with  $R_{\text{comp}} = 6 \times 10^8 \text{ cm}$  are smeared by up to 40 ms by the showers, suppressing periodic fluctuations of the backslash emission modulated with the spin of the MSP.

The orbital period  $P_{\text{orb}}$  is based on  $M_{\text{NS}}, M_{\text{comp}}$ , and  $a_{10}$  as  $P_{\text{orb}} = 2\pi \sqrt{R_{\text{orb}}^3 / (G[M_{\text{NS}} + M_{\text{comp}}])}$ , where

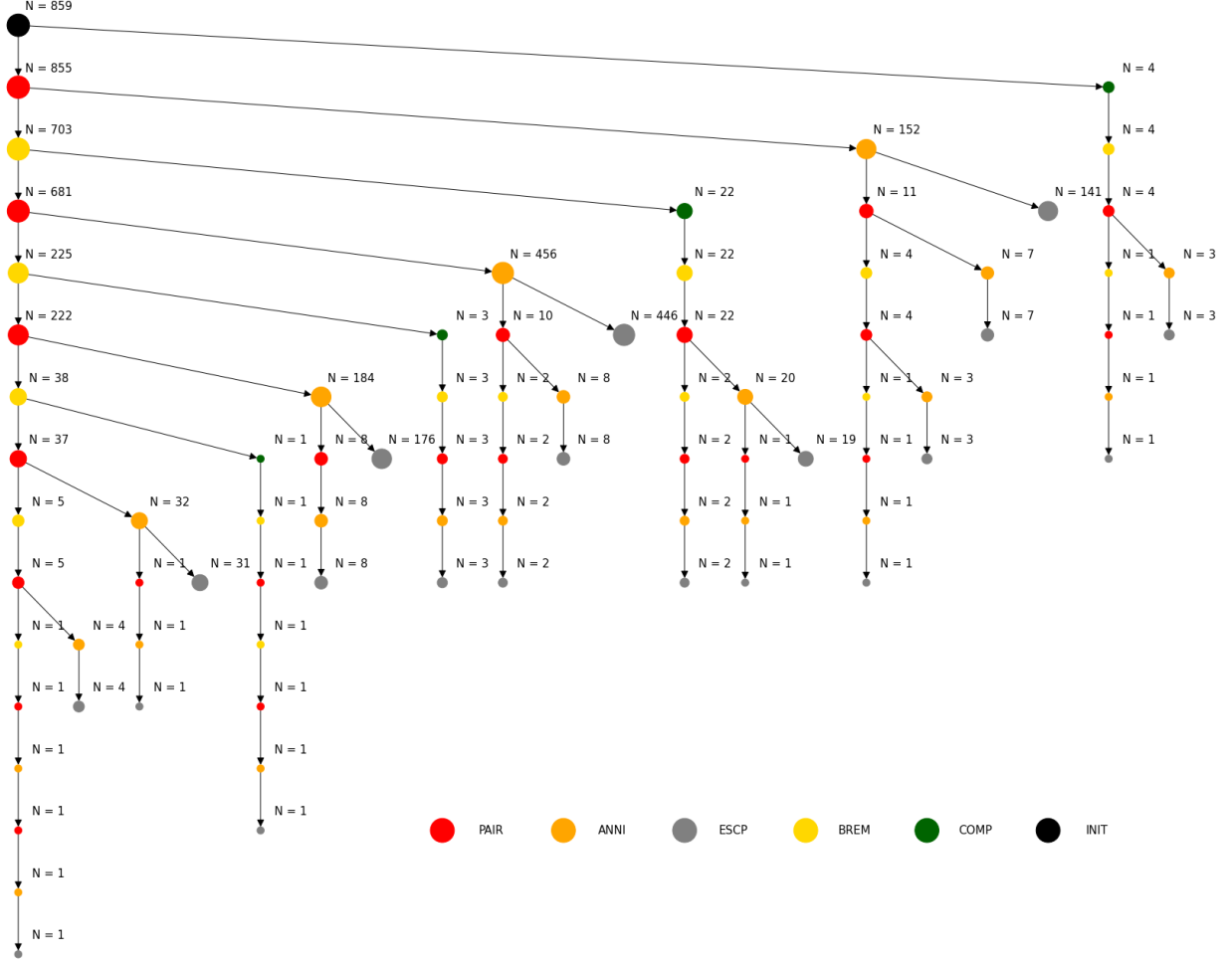


FIG. 8. This figure charts the evolution of 10,000 initial photons that result in escaping 511 keV photons for the C planet system. Each row is a generation and each branch represents a different path. The black vertex is the initial photon (INIT), green vertices are photons producing Compton scattered electrons (COMP), yellow vertices are electrons or positrons producing Bremsstrahlung photons (BREM), orange vertices are electron-positron annihilation to produce photons (ANNI), red vertices are photons producing electron-positron pairs (PAIR), and grey vertices are escaping 511 keV photons.

$R_{\text{orb}} = a_{10} \times 10^8$  m, and  $G$  is the gravitational constant. Most of the companion models have  $P_{\text{orb}} \sim 10^4$  s, except for the C WD model, which has  $P_{\text{orb}} \sim 10^3$  s. This is due to the large  $M_{\text{comp}}$  and small  $a_{10}$  of this model compared to the others.  $P_{\text{orb}}$  is listed in Table I for each model.



- T. Siegert, *Phys. Rev. D* **106**, 023030 (2022).
- [1] G. Vedrenne, J. P. Roques, V. Schönfelder, P. Mandrou, G. G. Lichti, A. von Kienlin, B. Cordier, S. Schanne, J. Knödlseeder, G. Skinner, P. Jean, F. Sanchez, P. Caraveo, B. Teegarden, P. von Ballmoos, L. Bouchet, P. Paul, J. Matteson, S. Boggs, C. Wunderer, P. Leleux, G. Weidenspointner, P. Durouchoux, R. Diehl, A. Strong, M. Cassé, M. A. Clair, and Y. André, *A&A* **411**, L63 (2003).
- [2] G. Skinner, R. Diehl, X.-L. Zhang, L. Bouchet, and P. Jean, *PoS Integral2014*, 054 (2015).
- [3] T. Siegert, R. Diehl, G. Khachatryan, M. G. H. Krause, F. Guglielmetti, J. Greiner, A. W. Strong, and X. Zhang, *A&A* **586**, A84 (2016), [arXiv:1512.00325 \[astro-ph.HE\]](https://arxiv.org/abs/1512.00325).
- [4] T. Siegert, *Positron-Annihilation Spectroscopy throughout the Milky Way*, Ph.D. thesis, Max-Planck-Institute for Extraterrestrial Physics, Garching (2017).
- [5] T. Siegert, *Astrophys. Space Sci.* **368**, 27 (2023), [arXiv:2303.15582 \[astro-ph.HE\]](https://arxiv.org/abs/2303.15582).
- [6] W. B. Atwood et al. (Fermi-LAT), *Astrophys. J.* **697**, 1071 (2009), [arXiv:0902.1089 \[astro-ph.IM\]](https://arxiv.org/abs/0902.1089).
- [7] M. Ackermann, M. Ajello, A. Albert, W. B. Atwood, L. Baldini, J. Ballet, G. Barbiellini, D. Bastieri, R. Bellazzini, E. Bissaldi, R. D. Blandford, E. D. Bloom, R. Bonino, E. Bottacini, T. J. Brandt, J. Bregeon, P. Bruel, R. Buehler, T. H. Burnett, R. A. Cameron, R. Caputo, M. Caragiulo, P. A. Caraveo, E. Cavazzuti, C. Cecchi, E. Charles, A. Chekhtman, J. Chiang, A. Chiappo, G. Chiaro, S. Ciprini, J. Conrad, F. Costanza, A. Cuomo, S. Cutini, F. D’Ammando, F. d. Palma, R. Desiante, S. W. Digel, N. D. Lalla, M. D. Mauro, L. D. Venere, P. S. Drell, C. Favuzzi, S. J. Fegan, E. C. Ferrara, W. B. Focke, A. Franckowiak, Y. Fukazawa, S. Funk, P. Fusco, F. Gargano, D. Gasparrini, N. Giglietto, F. Giordano, M. Giroletti, T. Glanzman, G. A. Gomez-Vargas, D. Green, I. A. Grenier, J. E. Grove, L. Guillemot, S. Guiriec, M. Gustafsson, A. K. Harding, E. Hays, J. W. Hewitt, D. Horan, T. Jogler, A. S. Johnson, T. Kamae, D. Kocovski, M. Kuss, G. L. Mura, S. Larsson, L. Latronico, J. Li, F. Longo, F. Loparco, M. N. Lovellette, P. Lubrano, J. D. Magill, S. Maldera, D. Malyshev, A. Manfreda, P. Martin, M. N. Mazziotta, P. F. Michelson, N. Mirabal, W. Mitthumsiri, T. Mizuno, A. A. Moiseev, M. E. Monzani, A. Morselli, M. Negro, E. Nuss, T. Ohsugi, M. Orienti, E. Orlando, J. F. Ormes, D. Paneque, J. S. Perkins, M. Persic, M. Pesce-Rollins, F. Piron, G. Principe, S. Rainò, R. Rando, M. Razzano, S. Razzaque, A. Reimer, O. Reimer, M. Sánchez-Conde, C. Sgrò, D. Simone, E. J. Siskind, F. Spada, G. Spandre, P. Spinelli, D. J. Suson, H. Tajima, K. Tanaka, J. B. Thayer, L. Tibaldo, D. F. Torres, E. Troja, Y. Uchiyama, G. Vianello, K. S. Wood, M. Wood, G. Zaharijas, and S. Zimmer, *The Astrophysical Journal* **840**, 43 (2017).
- [8] C. Keith and D. Hooper, *Physical Review D* **104** (2021), [10.1103/physrevd.104.063033](https://arxiv.org/abs/10.1103/physrevd.104.063033).
- [9] P. D. la Torre Luque, S. Balaji, and J. Silk, “New 511 keV line data provides strongest sub-gev dark matter constraints,” (2024), [arXiv:2312.04907 \[hep-ph\]](https://arxiv.org/abs/2312.04907).
- [10] J. Berteaud, F. Calore, J. Iguaz, P. D. Serpico, and T. Siegert, *Phys. Rev. D* **106**, 023030 (2022).
- [11] R. Bartels, F. Calore, E. Storm, and C. Weniger, *Monthly Notices of the Royal Astronomical Society* **480**, 3826 (2018), <https://academic.oup.com/mnras/article-pdf/480/3/3826/25520223/sty2135.pdf>.
- [12] R. Bartels, S. Krishnamurthy, and C. Weniger, *Physical Review Letters* **116** (2016), [10.1103/physrevlett.116.051102](https://arxiv.org/abs/10.1103/physrevlett.116.051102).
- [13] J. A. Tomsick, S. E. Boggs, A. Zoglauer, D. Hartmann, M. Ajello, E. Burns, C. Fryer, C. Karwin, C. Kierans, A. Lowell, J. Malzac, J. Roberts, P. Saint-Hilaire, A. Shih, T. Siegert, C. Sleator, T. Takahashi, F. Tavecchio, E. Wulf, J. Beechert, H. Gulick, A. Joens, H. Lazar, E. Neights, J. C. M. Oliveros, S. Matsumoto, T. Melia, H. Yoneda, M. Amman, D. Bal, P. von Ballmoos, H. Bates, M. Böttcher, A. Bulgarelli, E. Cavazzuti, H.-K. Chang, C. Chen, C.-Y. Chu, M. Corbelli, L. Costamante, L. Dreyer, V. Fioretti, F. Fenu, S. Gallego, G. Ghirlanda, E. Grove, C.-Y. Huang, P. Jean, N. Khatiya, J. Knödlseeder, M. Krause, M. Leising, T. R. Lewis, J. P. Lommler, L. Marcotulli, I. Martinez-Castellanos, S. Mittal, M. Negro, S. A. Nussirat, K. Nakazawa, U. Oberlack, D. Palmore, G. Panebianco, N. Parmiggiani, T. Parsotan, S. N. Pike, F. Rogers, H. Schutte, Y. Sheng, A. P. Smale, J. Smith, A. Trigg, T. Venters, Y. Watanabe, and H. Zhang, “The compton spectrometer and imager,” (2023), [arXiv:2308.12362 \[astro-ph.HE\]](https://arxiv.org/abs/2308.12362).
- [14] J. McEnery, J. A. Barrio, I. Agudo, M. Ajello, J.-M. Álvarez, S. Ansoldi, S. Anton, N. Auricchio, J. B. Stephen, L. Baldini, C. Bambi, M. Baring, U. Barres, D. Bastieri, J. Beacom, V. Beckmann, W. Bednarek, D. Bernard, E. Bissaldi, P. Blosler, H. Blumer, M. Boettcher, S. Boggs, A. Bolotnikov, E. Bottacini, V. Bozhilov, E. Bozzo, M. Briggs, J. Buckley, E. Burns, S. Busson, R. Campana, R. Caputo, M. Cardillo, E. Caroli, D. Castro, S. B. Cenko, E. Charles, W. Chen, T. Cheung, S. Ciprini, P. Coppi, R. C. da Silva, S. Cutini, F. D’Ammando, A. D. Angelis, M. D. Becker, G. D. Nolfo, S. D. Sordo, M. D. Mauro, L. D. Venere, S. Di- etrich, S. Digel, A. Dominguez, M. Doro, E. Ferrara, B. Fields, J. Finke, L. Foffano, C. Fryer, Y. Fukazawa, S. Funk, D. Gasparrini, J. Gelfand, M. Georganopoulos, F. Giordano, A. Giuliani, C. Gouiffes, B. Grefenstette, I. Grenier, S. Griffin, E. Grove, S. Guiriec, A. Harding, P. Harding, D. Hartmann, E. Hays, M. Hernanz, J. Hewitt, J. Holder, M. Hui, A. Inglis, R. Johnson, S. Jones, G. Kanbach, O. Kargaltsev, S. Kaufmann, M. Kerr, C. Kierans, F. Kislat, A. V. Klimentenko, J. Knödlseeder, D. Kocveski, J. Kopp, H. Krawczynsiki, J. Krizmanic, H. Kubo, N. K. Neilson, P. Laurent, J.-P. Lenain, H. Li, A. Lien, T. Linden, J. Lommler, F. Longo, M. Lovellette, M. López, A. Manousakis, L. Marcotulli, A. Marcowith, M. Martinez, M. McConnell, J. Metcalfe, E. Meyer, M. Meyer, R. Mignani, J. Mitchell, T. Mizuno, A. Moiseev, D. Morcuende, I. Moskalenko, M. Moss, K. Nakazawa, M. N. Mazziotta, U. Oberlack, M. Ohno, F. Oikonomou, R. Ojha, N. Omodei, E. Orlando, N. Otte, V. S. Paliya, L. Parker, B. Patricelli, J. Perkins, M. Petropoulou, C. Pittori, M. Pohl, T. Porter, E. Prandini, C. Prescod-Weinstein, J. Racusin, R. Rando, B. Rani, M. Ribó, J. Rodi, M. A. Sanchez-Conde, P. S. Parkinson, R. Schirato, P. Shawhan, C. Shrader, J. Smith, K. Smith,

- A. Stamerra, L. Stawarz, A. Strong, I. Stumke, H. Tajima, H. Takahashi, Y. Tanaka, V. Tatischeff, L.-S. The, D. Thompson, L. Tibaldo, J. Tomsick, L. Uhm, T. Venters, T. Vestrand, G. Vianello, Z. Wadiasingh, R. Walter, X. Wang, D. Williams, C. Wilson-Hodge, M. Wood, R. Woolf, E. Wulf, G. Younes, L. Zampieri, S. Zane, B. Zhang, H. Zhang, S. Zimmer, A. Zoglauer, and A. van der Horst, “[All-sky medium energy gamma-ray observatory: Exploring the extreme multimessenger universe,](#)” (2019), [arXiv:1907.07558 \[astro-ph.IM\]](#).
- [15] R. Caputo, M. Ajello, C. A. Kierans, J. S. Perkins, J. L. Racusin, L. Baldini, M. G. Baring, E. Bissaldi, E. Burns, N. Cannady, E. Charles, R. M. C. da Silva, K. Fang, H. Fleischhack, C. Fryer, Y. Fukazawa, J. E. Grove, D. Hartmann, E. J. Howell, M. Jadhav, C. M. Karwin, D. Kocevski, N. Kurahashi, L. Latronico, T. R. Lewis, R. Leys, A. Lien, L. Marcotulli, I. Martinez-Castellanos, M. N. Mazziotta, J. McEnery, J. Metcalfe, K. Murase, M. Negro, L. Parker, B. Philips, C. Prescod-Weinstein, S. Razzaque, P. S. Shawhan, Y. Sheng, T. A. Shutt, D. Shy, C. Sleator, A. L. Steinhebel, N. Striebig, Y. Suda, D. Tak, H. Tajima, J. Valverde, T. M. Venters, Z. Wadiasingh, R. S. Woolf, E. A. Wulf, H. Zhang, and A. Zoglauer, *Journal of Astronomical Telescopes, Instruments, and Systems* **8** (2022), [10.1117/1.jatis.8.4.044003](#).
- [16] E. Orlando, E. Bottacini, A. Moiseev, A. Bodaghee, W. Collmar, T. Ensslin, I. V. Moskalenko, M. Negro, S. Profumo, S. W. Digel, D. J. Thompson, M. G. Baring, A. Bolotnikov, N. Cannady, G. A. Carini, V. Eberle, I. A. Grenier, A. K. Harding, D. Hartmann, S. Herrmann, M. Kerr, R. Krivonos, P. Laurent, F. Longo, A. Morselli, B. Phillips, M. Sasaki, P. Shawhan, D. Shy, G. Skinner, L. D. Smith, F. W. Stecker, A. Strong, S. Sturmer, J. A. Tomsick, Z. Wadiasingh, R. S. Woolf, E. Yates, K.-P. Ziock, and A. Zoglauer, *Journal of Cosmology and Astroparticle Physics* **2022**, 036 (2022).
- [17] T. Aramaki, P. O. H. Adrian, G. Karagiorgi, and H. Odaka, *Astroparticle Physics* **114**, 107–114 (2020).
- [18] T. Shutt, B. Trbalic, E. Charles, N. D. Lalla, O. Hitchcock, S. Jett, R. Linehan, S. Luitz, G. Madejski, A. Peña-Perez, and Y.-T. Tsai, “[The gammatpc gamma-ray telescope concept,](#)” (2025), [arXiv:2502.14841 \[astro-ph.IM\]](#).
- [19] J. Buckley, Adapt, S. Alussirat, C. Altomare, R. G. Bose, D. L. Braun, J. H. Buckley, J. Buhler, E. Burns, R. D. Chamberlain, W. Chen, M. L. Cherry, L. Di Venere, J. Dumonthier, M. Errando, S. Funk, F. Giordano, J. Hoffman, Z. Hughes, D. J. Huth, P. L. Kelly, J. F. Krizmanic, M. Kuwahara, F. Licciulli, G. Liu, M. N. Mazziotta, J. G. Mitchell, J. W. Mitchell, G. A. de Nolfo, R. Paoletti, R. Pillera, B. F. Rauch, D. Serini, G. E. Simburger, M. Sudvarg, G. Suarez, T. Tatoli, G. S. Varner, E. A. Wulf, A. Zink, and W. V. Zober, in *37th International Cosmic Ray Conference* (2022) p. 655.
- [20] M. A. Alpar, A. F. Cheng, M. A. Ruderman, and J. Shaham, *Nature* **300**, 728 (1982).
- [21] D. J. Helfand, M. A. Ruderman, and J. Shaham, *Nature* **304**, 423 (1983).
- [22] D. Bhattacharya and E. van den Heuvel, *Physics Reports* **203**, 1 (1991).
- [23] T. M. Tauris and G. J. Savonije, *A&A* **350**, 928 (1999), [arXiv:astro-ph/9909147 \[astro-ph\]](#).
- [24] D. A. Smith, S. Abdollahi, M. Ajello, M. Bailes, L. Baldini, J. Ballet, M. G. Baring, C. Bassa, J. B. Gonzalez, R. Bellazzini, A. Berretta, B. Bhattacharyya, E. Bissaldi, R. Bonino, E. Bottacini, J. Bregeon, P. Bruel, M. Burgay, T. H. Burnett, R. A. Cameron, F. Camilo, R. Caputo, P. A. Caraveo, E. Cavazzuti, G. Chiaro, S. Ciprini, C. J. Clark, I. Cognard, A. Corongiu, P. C. Orestano, M. Crnogorčević, A. Cuoco, S. Cutini, F. D’Ammando, A. de Angelis, M. E. DeCesar, S. De Gaetano, R. de Menezes, J. Deneva, F. de Palma, N. Di Lalla, F. Dirrsa, L. Di Venere, A. Domínguez, D. Dumora, S. J. Fegan, E. C. Ferrara, A. Fiori, H. Fleischhack, C. Flynn, A. Franckowiak, P. C. C. Freire, Y. Fukazawa, P. Fusco, G. Galanti, V. Gammaldi, F. Gargano, D. Gasparrini, F. Giacchino, N. Giglietto, F. Giordano, M. Giroletti, D. Green, I. A. Grenier, L. Guillemot, S. Guiriec, M. Gustafsson, A. K. Harding, E. Hays, J. W. Hewitt, D. Horan, X. Hou, F. Jankowski, R. P. Johnson, T. J. Johnson, S. Johnston, J. Kataoka, M. J. Keith, M. Kerr, M. Kramer, M. Kuss, L. Latronico, S.-H. Lee, D. Li, J. Li, B. Limyansky, F. Longo, F. Loparco, L. Lorusso, M. N. Lovellette, M. Lower, P. Lubrano, A. G. Lyne, Y. Maan, S. Maldera, R. N. Manchester, A. Manfreda, M. Marelli, G. Martí-Devesa, M. N. Mazziotta, J. E. McEnery, I. Mereu, P. F. Michelson, M. Mickaliger, W. Mitthumsiri, T. Mizuno, A. A. Moiseev, M. E. Monzani, A. Morselli, M. Negro, R. Nemmen, L. Nieder, E. Nuss, N. Omodei, M. Orienti, E. Orlando, J. F. Ormes, M. Palatiello, D. Paneque, G. Panzarini, A. Parthasarathy, M. Perisic, M. Pesce-Rollins, R. Pillera, H. Poon, T. A. Porter, A. Possenti, G. Principe, S. Rainò, R. Rando, S. M. Ransom, P. S. Ray, M. Razzano, S. Razzaque, A. Reimer, O. Reimer, N. Renault-Tinacci, R. W. Romani, M. Sánchez-Conde, P. M. S. Parkinson, L. Scotton, D. Serini, C. Sgrò, R. Shannon, V. Sharma, Z. Shen, E. J. Siskind, G. Spandre, P. Spinelli, B. W. Stappers, T. E. Stephens, D. J. Suson, S. Tabassum, H. Tajima, D. Tak, G. Theureau, D. J. Thompson, O. Tibolla, D. F. Torres, J. Valverde, C. Venter, Z. Wadiasingh, N. Wang, N. Wang, P. Wang, P. Weltevrede, K. Wood, J. Yan, G. Zaharijas, C. Zhang, and W. Zhu, *The Astrophysical Journal* **958**, 191 (2023).
- [25] I. Contopoulos, D. Kazanas, and C. Fendt, *ApJ* **511**, 351 (1999), [arXiv:astro-ph/9903049 \[astro-ph\]](#).
- [26] I. Contopoulos and C. Kalapotharakos, *MNRAS* **404**, 767 (2010), [arXiv:0912.2369 \[astro-ph.HE\]](#).
- [27] X.-N. Bai and A. Spitkovsky, *ApJ* **715**, 1282 (2010), [arXiv:0910.5741 \[astro-ph.HE\]](#).
- [28] C. Kalapotharakos, A. K. Harding, and D. Kazanas, *ApJ* **793**, 97 (2014), [arXiv:1310.3545 \[astro-ph.HE\]](#).
- [29] B. Cerutti, A. A. Philippov, and A. Spitkovsky, *MNRAS* **457**, 2401 (2016), [arXiv:1511.01785 \[astro-ph.HE\]](#).
- [30] C. Kalapotharakos, A. K. Harding, D. Kazanas, and G. Brambilla, *ApJ* **842**, 80 (2017), [arXiv:1702.03069 \[astro-ph.HE\]](#).
- [31] C. Kalapotharakos, G. Brambilla, A. Timokhin, A. K. Harding, and D. Kazanas, *ApJ* **857**, 44 (2018), [arXiv:1710.03170 \[astro-ph.HE\]](#).
- [32] A. A. Philippov and A. Spitkovsky, *ApJ* **855**, 94 (2018), [arXiv:1707.04323 \[astro-ph.HE\]](#).
- [33] G. Cao and X. Yang, *ApJ* **874**, 166 (2019), [arXiv:1903.01694 \[astro-ph.HE\]](#).
- [34] C. Kalapotharakos, Z. Wadiasingh, A. K. Harding, and

- D. Kazanas, *ApJ* **954**, 204 (2023), [arXiv:2303.04054 \[astro-ph.HE\]](#).
- [35] B. Cerutti, E. Figueiredo, and G. Dubus, *arXiv e-prints*, [arXiv:2412.02307 \(2024\)](#), [arXiv:2412.02307 \[astro-ph.HE\]](#).
- [36] A. Wolszczan and D. A. Frail, *Nature* **355**, 145 (1992).
- [37] P. F. Wang, J. L. Han, Z. L. Yang, T. Wang, C. Wang, W. Q. Su, J. Xu, D. J. Zhou, Y. Yan, W. C. Jing, N. N. Cai, J. P. Yuan, R. X. Xu, H. G. Wang, and X. P. You, “The fast galactic plane pulsar snapshot survey: VIII. 112 binary pulsars,” (2024), [arXiv:2412.03062 \[astro-ph.HE\]](#).
- [38] M. S. E. Roberts, in *Radio Pulsars: An Astrophysical Key to Unlock the Secrets* (American Institute of Physics Conference Series, Vol. 1357, edited by M. Burgay, N. D’Amico, P. Esposito, A. Pellizzoni, and A. Possenti (AIP, 2011) pp. 127–130, [arXiv:1103.0819 \[astro-ph.HE\]](#)).
- [39] M. S. E. Roberts, in *Neutron Stars and Pulsars: Challenges and Opportunities after 80 years* (IAU Symposium, Vol. 291, edited by J. van Leeuwen (2013) pp. 127–132, [arXiv:1210.6903 \[astro-ph.HE\]](#)).
- [40] M. H. van Kerkwijk, R. P. Breton, and S. R. Kulkarni, *ApJ* **728**, 95 (2011), [arXiv:1009.5427 \[astro-ph.HE\]](#).
- [41] M. Linares, T. Shahbaz, and J. Casares, *ApJ* **859**, 54 (2018), [arXiv:1805.08799 \[astro-ph.HE\]](#).
- [42] J. Strader, S. Swihart, L. Chomiuk, A. Bahramian, C. Britt, C. C. Cheung, K. Dage, J. Halpern, K.-L. Li, R. P. Mignani, J. A. Orosz, M. Peacock, R. Salinas, L. Shishkovsky, and E. Tremou, *ApJ* **872**, 42 (2019), [arXiv:1812.04626 \[astro-ph.HE\]](#).
- [43] S. J. Swihart, J. Strader, L. Chomiuk, E. Aydi, K. V. Sokolovsky, P. S. Ray, and M. Kerr, *ApJ* **941**, 199 (2022), [arXiv:2210.16295 \[astro-ph.HE\]](#).
- [44] J. A. Simpson, M. Linares, J. Casares, T. Shahbaz, B. Sen, and F. Camilo, *MNRAS* **536**, 2169 (2025), [arXiv:2408.11099 \[astro-ph.HE\]](#).
- [45] A. Mucciarelli, M. Salaris, B. Lanzoni, C. Pallanca, E. Dalessandro, and F. R. Ferraro, *ApJL* **772**, L27 (2013), [arXiv:1307.0919 \[astro-ph.SR\]](#).
- [46] R. W. Romani, A. V. Filippenko, and S. B. Cenko, *ApJ* **804**, 115 (2015), [arXiv:1503.05247 \[astro-ph.HE\]](#).
- [47] T. Shahbaz, J. I. González-Hernández, R. P. Breton, M. R. Kennedy, D. Mata Sánchez, and M. Linares, *MNRAS* **513**, 71 (2022), [arXiv:2202.09070 \[astro-ph.HE\]](#).
- [48] S. M. Ransom, I. H. Stairs, A. M. Archibald, J. W. T. Hessels, D. L. Kaplan, M. H. van Kerkwijk, J. Boyles, A. T. Deller, S. Chatterjee, A. Schechtman-Rook, A. Berndsen, R. S. Lynch, D. R. Lorimer, C. Karako-Argaman, V. M. Kaspi, V. I. Kondratiev, M. A. McLaughlin, J. van Leeuwen, R. Rosen, M. S. E. Roberts, and K. Stovall, *Nature* **505**, 520 (2014), [arXiv:1401.0535 \[astro-ph.SR\]](#).
- [49] L. Nieder, M. Kerr, C. J. Clark, P. Bruel, H. T. Cromartie, S. M. Ransom, and P. S. Ray, *ApJL* **931**, L3 (2022), [arXiv:2202.05482 \[astro-ph.HE\]](#).
- [50] A. Patruno and M. Kama, *Astronomy & Astrophysics* **608**, A147 (2017).
- [51] S. Sigurdsson, H. B. Richer, B. M. Hansen, I. H. Stairs, and S. E. Thorsett, *Science* **301**, 193 (2003), [arXiv:astro-ph/0307339 \[astro-ph\]](#).
- [52] M. Bailes, S. D. Bates, V. Bhalerao, N. D. R. Bhat, M. Burgay, S. Burke-Spolaor, N. D’Amico, S. Johnston, M. J. Keith, M. Kramer, S. R. Kulkarni, L. Levin, A. G. Lyne, S. Milia, A. Possenti, L. Spitler, B. Stappers, and W. van Straten, *Science* **333**, 1717–1720 (2011).
- [53] H. M. Johnston and S. R. Kulkarni, *ApJ* **368**, 504 (1991).
- [54] B. C. Andersen and S. M. Ransom, *ApJL* **863**, L13 (2018), [arXiv:1807.07900 \[astro-ph.HE\]](#).
- [55] N. Pol, M. McLaughlin, D. R. Lorimer, and N. Garver-Daniels, *The Astrophysical Journal* **912**, 22 (2021).
- [56] C. J. Clark, J. Wu, H. J. Pletsch, L. Guillemot, B. Allen, C. Aulbert, C. Beer, O. Bock, A. Cuéllar, H. B. Eggenstein, H. Fehrmann, M. Kramer, B. Machenschalk, and L. Nieder, *ApJ* **834**, 106 (2017), [arXiv:1611.01015 \[astro-ph.HE\]](#).
- [57] L. Nieder, B. Allen, C. J. Clark, and H. J. Pletsch, *ApJ* **901**, 156 (2020), [arXiv:2004.11740 \[astro-ph.HE\]](#).
- [58] L. Nieder, C. J. Clark, D. Kandel, R. W. Romani, C. G. Bassa, B. Allen, A. Ashok, I. Cognard, H. Fehrmann, P. Freire, R. Karuppusamy, M. Kramer, D. Li, B. Machenschalk, Z. Pan, M. A. Papa, S. M. Ransom, S. Ray, J. Roy, P. Wang, J. Wu, C. Aulbert, E. D. Barr, B. Beheshtipour, O. Behnke, B. Bhattacharyya, R. P. Breton, F. Camilo, C. Choquet, V. S. Dhillon, E. C. Ferrara, L. Guillemot, J. W. T. Hessels, M. Kerr, S. A. Kwang, T. R. Marsh, M. B. Mickaliger, Z. Pleunis, H. J. Pletsch, M. S. E. Roberts, S. Sanpa-arsa, and B. Steltner, *ApJL* **902**, L46 (2020), [arXiv:2009.01513 \[astro-ph.HE\]](#).
- [59] L. M. van Haften, G. Nelemans, R. Voss, S. Toonen, S. F. Portegies Zwart, L. R. Yungelson, and M. V. van der Sluys, *A&A* **552**, A69 (2013), [arXiv:1302.7181 \[astro-ph.SR\]](#).
- [60] P. Amaro-Seoane, H. Audley, S. Babak, J. Baker, E. Barausse, P. Bender, E. Berti, P. Binetruy, M. Born, D. Bortoluzzi, J. Camp, C. Caprini, V. Cardoso, M. Colpi, J. Conklin, N. Cornish, C. Cutler, K. Danzmann, R. Dolesi, L. Ferraioli, V. Ferroni, E. Fitzsimons, J. Gair, L. G. Bote, D. Giardini, F. Gibert, C. Grimani, H. Halloin, G. Heinzel, T. Hertog, M. Hewitson, K. Holley-Bockelmann, D. Hollington, M. Hueller, H. Inchauspe, P. Jetzer, N. Karnesis, C. Killow, A. Klein, B. Klipstein, N. Korsakova, S. L. Larson, J. Livas, I. Lloro, N. Man, D. Mance, J. Martino, I. Mateos, K. McKenzie, S. T. McWilliams, C. Miller, G. Mueller, G. Nardini, G. Nelemans, M. Nofrarias, A. Petiteau, P. Pivato, E. Plagnol, E. Porter, J. Reiche, D. Robertson, N. Robertson, E. Rossi, G. Rusano, B. Schutz, A. Sesana, D. Shoemaker, J. Slutsky, C. F. Sopuerta, T. Sumner, N. Tamanini, I. Thorpe, M. Troebs, M. Vallisneri, A. Vecchio, D. Vetrugno, S. Vitale, M. Volonteri, G. Wanner, H. Ward, P. Wass, W. Weber, J. Ziemer, and P. Zweifel, “*Laser interferometer space antenna*,” (2017), [arXiv:1702.00786 \[astro-ph.IM\]](#).
- [61] M. Colpi, K. Danzmann, M. Hewitson, K. Holley-Bockelmann, P. Jetzer, G. Nelemans, A. Petiteau, D. Shoemaker, C. Sopuerta, R. Stebbins, N. Tanvir, H. Ward, W. J. Weber, I. Thorpe, A. Dauriskikh, A. Deep, I. F. Núñez, C. G. Marirrosi, M. Gehler, J.-P. Halain, O. Jennrich, U. Lammers, J. Larrañaga, M. Lieser, N. Lützgendorf, W. Martens, L. Mondin, A. P. Niño, P. Amaro-Seoane, M. A. Sedda, P. Auclair, S. Babak, Q. Baghi, V. Baibhav, T. Baker, J.-B. Bayle, C. Berry, E. Berti, G. Boileau, M. Bonetti, R. Brito, R. Busicchio, G. Calcagni, P. R. Capelo, C. Caprini,

- A. Caputo, E. Castelli, H.-Y. Chen, X. Chen, A. Chua, G. Davies, A. Derdzinski, V. F. Domcke, D. Doneva, I. Dvorkin, J. M. Ezquiaga, J. Gair, Z. Haiman, I. Harry, O. Hartwig, A. Hees, A. Heffernan, S. Husa, D. Izquierdo, N. Karnesis, A. Klein, V. Korol, N. Korsakova, T. Kupfer, D. Laghi, A. Lamberts, S. Larson, M. L. Jeune, M. Lewicki, T. Littenberg, E. Madge, A. Mangiagli, S. Marsat, I. M. Vilchez, A. Maselli, J. Mathews, M. van de Meent, M. Muratore, G. Nardini, P. Pani, M. Peloso, M. Pieroni, A. Pound, H. Quelquejay-Leclere, A. Ricciardone, E. M. Rossi, A. Sartirana, E. Savalle, L. Sberna, A. Sesana, D. Shoemaker, J. Slutsky, T. Sotiriou, L. Speri, M. Staab, D. Steer, N. Tamanini, G. Tasinato, J. Torrado, A. Torres-Orjuela, A. Toubiana, M. Vallisneri, A. Vecchio, M. Volonteri, K. Yagi, and L. Zwick, “*Lisa definition study report*,” (2024), [arXiv:2402.07571](https://arxiv.org/abs/2402.07571) [[astro-ph.CO](https://arxiv.org/abs/2402.07571)].
- [62] T. M. Tauris, *Physical Review Letters* **121** (2018), [10.1103/physrevlett.121.131105](https://doi.org/10.1103/physrevlett.121.131105).
- [63] W.-C. Chen, D.-D. Liu, and B. Wang, *The Astrophysical Journal Letters* **900**, L8 (2020).
- [64] K. Breivik, “*Population synthesis of gravitational wave sources*,” (2025), [arXiv:2502.03523](https://arxiv.org/abs/2502.03523) [[astro-ph.HE](https://arxiv.org/abs/2502.03523)].
- [65] G. Nelemans, L. R. Yungelson, and S. F. Portegies Zwart, *Astronomy & Astrophysics* **375**, 890–898 (2001).
- [66] J. Liu and Y. Zhang, *Publications of the Astronomical Society of the Pacific* **126**, 211–218 (2014).
- [67] K. Breivik, S. Coughlin, M. Zevin, C. L. Rodriguez, K. Kremer, C. S. Ye, J. J. Andrews, M. Kurkowski, M. C. Digman, S. L. Larson, and F. A. Rasio, *The Astrophysical Journal* **898**, 71 (2020).
- [68] J. H. Krolik and M. W. Sincell, *ApJ* **357**, 208 (1990).
- [69] A. M. Hillas, *Nature* **312**, 50 (1984).
- [70] A. Zoglauer et al., *New Astr. News* **50**, 629 (2006).
- [71] S. Agostinelli, J. Allison, K. Amako, J. Apostolakis, H. Araujo, P. Arce, M. Asai, D. Axen, S. Banerjee, G. Barrand, F. Behner, L. Bellagamba, J. Boudreau, L. Broglia, A. Brunengo, H. Burkhardt, S. Chauvie, J. Chuma, R. Chytracek, G. Cooperman, G. Cosmo, P. Degtyarenko, A. Dell’Acqua, G. Depaola, D. Dietrich, R. Enami, A. Feliciello, C. Ferguson, H. Fesefeldt, G. Folger, F. Foppiano, A. Forti, S. Garelli, S. Giani, R. Giannitrapani, D. Gibin, J. Gómez Cadenas, I. González, G. Gracia Abril, G. Greeniaus, W. Greiner, V. Grichine, A. Grossheim, S. Guatelli, P. Gumplinger, R. Hamatsu, K. Hashimoto, H. Hasui, A. Heikkinen, A. Howard, V. Ivanchenko, A. Johnson, F. Jones, J. Kallenbach, N. Kanaya, M. Kawabata, Y. Kawabata, M. Kawaguti, S. Kelner, P. Kent, A. Kimura, T. Kodama, R. Kokoulin, M. Kossov, H. Kurashige, E. Lamanna, T. Lampén, V. Lara, V. Lefebure, F. Lei, M. Liendl, W. Lockman, F. Longo, S. Magni, M. Maire, E. Medernach, K. Minamimoto, P. Mora de Freitas, Y. Morita, K. Murakami, M. Nagamatu, R. Nartallo, P. Nieminen, T. Nishimura, K. Ohtsubo, M. Okamura, S. O’Neale, Y. Oohata, K. Paech, J. Perl, A. Pfeiffer, M. Pia, F. Ranjard, A. Rybin, S. Sadilov, E. Di Salvo, G. Santin, T. Sasaki, N. Savvas, Y. Sawada, S. Scherer, S. Sei, V. Sirotenko, D. Smith, N. Starkov, H. Stoecker, J. Sulkimo, M. Takahata, S. Tanaka, E. Tcherniaev, E. Safai Tehrani, M. Tropeano, P. Truscott, H. Uno, L. Urban, P. Urban, M. Verderi, A. Walkden, W. Wander, H. Weber, J. Wellisch, T. Wenaus, D. Williams, D. Wright, T. Yamada, H. Yoshida, and D. Zschiesche, *Nuclear Instruments and Methods in Physics Research Section A: Accelerators, Spectrometers, Detectors and Associated Equipment* **506**, 250 (2003).
- [72] M. Berger, J. Coursey, M. Zucker, and J. Chang, “*Stopping-power & range tables for electrons, protons, and helium ions*,” (2017).
- [73] A. K. Harding and A. G. Muslimov, *ApJ* **743**, 181 (2011), [arXiv:1111.1668](https://arxiv.org/abs/1111.1668) [[astro-ph.HE](https://arxiv.org/abs/1111.1668)].
- [74] A. K. Harding, C. Kalapotharakos, M. Barnard, and C. Venter, *ApJL* **869**, L18 (2018), [arXiv:1811.11157](https://arxiv.org/abs/1811.11157) [[astro-ph.HE](https://arxiv.org/abs/1811.11157)].
- [75] H. E. S. S. Collaboration, F. Aharonian, F. Ait Benkhali, J. Aschersleben, H. Ashkar, M. Backes, V. Barbosa Martins, R. Batzofin, Y. Becherini, D. Berge, K. Bernlöhr, B. Bi, M. Böttcher, C. Boisson, J. Bolmont, M. de Bony de Lavergne, J. Borowska, F. Bradascio, M. Breuhaus, R. Brose, F. Brun, B. Bruno, T. Bulik, C. Burger-Scheidlin, T. Bylund, F. Cangemi, S. Caroff, S. Casanova, J. Celic, M. Ceruti, T. Chand, S. Chandra, A. Chen, O. Chibueze, G. Cotter, J. Damascene Mbarubucyeye, A. Djannati-Ataï, A. Dmytriiev, K. Egberts, J. P. Ernenwein, K. Feijen, A. Fiasson, G. Fichtel de Clairfontaine, G. Fontaine, M. Fülling, S. Funk, S. Gabici, Y. A. Gallant, S. Ghafourizadeh, G. Giavitto, L. Giunti, D. Glawion, J. F. Glicenstein, P. Goswami, G. Grolleron, M. H. Grondin, L. Haerer, M. Haupt, J. A. Hinton, W. Hofmann, T. L. Holch, M. Holler, D. Horns, Z. Huang, M. Jamrozny, F. Jankowsky, V. Joshi, I. Jung-Richardt, E. Kasai, K. Katarzyński, B. Khélifi, S. Klepser, W. Kluźniak, N. Komin, K. Kosack, D. Kostunin, R. G. Lang, S. Le Stum, A. Lemièrre, M. Lemoine-Goumard, J. P. Lenain, F. Leuschner, T. Lohse, A. Luashvili, I. Lypova, J. Mackey, D. Malyshev, D. Malyshev, V. Marandon, P. Marchegiani, A. Marcowith, P. Marinos, G. Martí-Devesa, R. Marx, G. Maurin, M. Meyer, A. Mitchell, R. Moderski, L. Mohrmann, A. Montanari, E. Moulin, J. Muller, T. Murach, K. Nakashima, M. de Naurois, J. Niemiec, A. P. Noel, P. O’Brien, S. Ohm, L. Olivera-Nieto, E. de Ona Wilhelmi, M. Ostrowski, S. Panny, M. Panter, R. D. Parsons, G. Peron, S. Pita, D. A. Prokhorov, H. Prokoph, G. Pühlhofer, M. Punch, A. Quirrenbach, P. Reichherzer, A. Reimer, O. Reimer, M. Renaud, F. Rieger, G. Rowell, B. Rudak, E. Ruiz-Velasco, V. Sahakian, S. Sailer, H. Salzmann, D. A. Sanchez, A. Santangelo, M. Sasaki, F. Schüssler, U. Schwanke, J. N. S. Shapopi, A. Sinha, H. Sol, A. Specovius, S. Spencer, M. Spir-Jacob, L. Stawarz, R. Steenkamp, S. Steinmassl, C. Steppa, I. Sushch, H. Suzuki, T. Takahashi, T. Tanaka, T. Tavernier, R. Terrier, C. Thorpe-Morgan, M. Tluczykont, M. Tsirou, N. Tsuji, C. van Eldik, M. Vecchi, J. Veh, C. Venter, J. Vink, S. J. Wagner, F. Werner, R. White, A. Wierzcholska, Y. Wun Wong, H. Yassin, M. Zacharias, D. Zargaryan, A. A. Zdziarski, A. Zech, S. J. Zhu, S. Zouari, N. Żywucka, R. Zanin, M. Kerr, S. Johnston, R. M. Shannon, and D. A. Smith, *Nature Astronomy* **7**, 1341 (2023), [arXiv:2310.06181](https://arxiv.org/abs/2310.06181) [[astro-ph.HE](https://arxiv.org/abs/2310.06181)].
- [76] C. Guépin, B. Cerutti, and K. Kotera, *A&A* **635**, A138 (2020), [arXiv:1910.11387](https://arxiv.org/abs/1910.11387) [[astro-ph.HE](https://arxiv.org/abs/1910.11387)].
- [77] Z. Wadiasingh, A. K. Harding, C. Venter,

- M. Böttcher, and M. G. Baring, *ApJ* **839**, 80 (2017), [arXiv:1703.09560 \[astro-ph.HE\]](#).
- [78] C. J. T. van der Merwe, Z. Wadiasingh, C. Venter, A. K. Harding, and M. G. Baring, *ApJ* **904**, 91 (2020), [arXiv:2010.01125 \[astro-ph.HE\]](#).
- [79] M. Sim, H. An, and Z. Wadiasingh, *ApJ* **964**, 109 (2024), [arXiv:2402.02674 \[astro-ph.HE\]](#).
- [80] R. N. Manchester, G. B. Hobbs, A. Teoh, and M. Hobbs, *The Astronomical Journal* **129**, 1993–2006 (2005).
- [81] K. I. I. Koljonen, S. S. Lindseth, M. Linares, A. K. Harding, and M. Turchetta, *Monthly Notices of the Royal Astronomical Society* **529**, 575 (2024), <https://academic.oup.com/mnras/article-pdf/529/1/575/57178779/stae498.pdf>.
- [82] J. M. Rankin, *ApJ* **352**, 247 (1990).
- [83] P. L. Gonthier, A. K. Harding, E. C. Ferrara, S. E. Frederick, V. E. Mohr, and Y.-M. Koh, *ApJ* **863**, 199 (2018), [arXiv:1806.11215 \[astro-ph.HE\]](#).
- [84] T. Robson, N. J. Cornish, and C. Liu, *Classical and Quantum Gravity* **36**, 105011 (2019).
- [85] P. P. Eggleton, *ApJ* **268**, 368 (1983).
- [86] B. Paxton, L. Bildsten, A. Dotter, F. Herwig, P. Lesaffre, and F. Timmes, *ApJS* **192**, 3 (2011), [arXiv:1009.1622 \[astro-ph.SR\]](#).
- [87] B. Paxton, M. Cantiello, P. Arras, L. Bildsten, E. F. Brown, A. Dotter, C. Mankovich, M. H. Montgomery, D. Stello, F. X. Timmes, and R. Townsend, *ApJS* **208**, 4 (2013), [arXiv:1301.0319 \[astro-ph.SR\]](#).
- [88] B. Paxton, P. Marchant, J. Schwab, E. B. Bauer, L. Bildsten, M. Cantiello, L. Dessart, R. Farmer, H. Hu, N. Langer, R. H. D. Townsend, D. M. Townsley, and F. X. Timmes, *ApJS* **220**, 15 (2015), [arXiv:1506.03146 \[astro-ph.SR\]](#).
- [89] B. Paxton, J. Schwab, E. B. Bauer, L. Bildsten, S. Blinnikov, P. Duffell, R. Farmer, J. A. Goldberg, P. Marchant, E. Sorokina, A. Thoul, R. H. D. Townsend, and F. X. Timmes, *ApJS* **234**, 34 (2018), [arXiv:1710.08424 \[astro-ph.SR\]](#).
- [90] B. Paxton, R. Smolec, J. Schwab, A. Gautschy, L. Bildsten, M. Cantiello, A. Dotter, R. Farmer, J. A. Goldberg, A. S. Jermyn, S. M. Kanbur, P. Marchant, A. Thoul, R. H. D. Townsend, W. M. Wolf, M. Zhang, and F. X. Timmes, *ApJS* **243**, 10 (2019), [arXiv:1903.01426 \[astro-ph.SR\]](#).
- [91] A. S. Jermyn, E. B. Bauer, J. Schwab, R. Farmer, W. H. Ball, E. P. Bellinger, A. Dotter, M. Joyce, P. Marchant, J. S. G. Mombarg, W. M. Wolf, T. L. Sunny Wong, G. C. Cinquegrana, E. Farrell, R. Smolec, A. Thoul, M. Cantiello, F. Herwig, O. Toloza, L. Bildsten, R. H. D. Townsend, and F. X. Timmes, *ApJS* **265**, 15 (2023), [arXiv:2208.03651 \[astro-ph.SR\]](#).
- [92] F. J. Rogers and A. Nayfonov, *ApJ* **576**, 1064 (2002).
- [93] D. Saumon, G. Chabrier, and H. M. van Horn, *ApJS* **99**, 713 (1995).
- [94] A. W. Irwin, “The freeeos code for calculating the equation of state for stellar interiors,” (2004).
- [95] F. X. Timmes and F. D. Swesty, *ApJS* **126**, 501 (2000).
- [96] A. Y. Potekhin and G. Chabrier, *Contributions to Plasma Physics* **50**, 82 (2010), [arXiv:1001.0690 \[physics.plasm-ph\]](#).
- [97] A. S. Jermyn, J. Schwab, E. Bauer, F. X. Timmes, and A. Y. Potekhin, *ApJ* **913**, 72 (2021), [arXiv:2104.00691 \[astro-ph.SR\]](#).
- [98] C. A. Iglesias and F. J. Rogers, *ApJ* **412**, 752 (1993).
- [99] C. A. Iglesias and F. J. Rogers, *ApJ* **464**, 943 (1996).
- [100] J. W. Ferguson, D. R. Alexander, F. Allard, T. Barman, J. G. Bodnarik, P. H. Hauschildt, A. Heffner-Wong, and A. Tamanai, *ApJ* **623**, 585 (2005), [astro-ph/0502045](#).
- [101] J. Poutanen, *ApJ* **835**, 119 (2017), [arXiv:1606.09466 \[astro-ph.HE\]](#).
- [102] S. Cassisi, A. Y. Potekhin, A. Pietrinferni, M. Cate-lan, and M. Salaris, *ApJ* **661**, 1094 (2007), [astro-ph/0703011](#).
- [103] S. Blouin, N. R. Shaffer, D. Saumon, and C. E. Starrett, *ApJ* **899**, 46 (2020), [arXiv:2006.16390 \[astro-ph.SR\]](#).
- [104] R. H. Cyburt, A. M. Amthor, R. Ferguson, Z. Meisel, K. Smith, S. Warren, A. Heger, R. D. Hoffman, T. Rauscher, A. Sakharuk, H. Schatz, F. K. Thiele-mann, and M. Wiescher, *ApJS* **189**, 240 (2010).
- [105] C. Angulo, M. Arnould, M. Rayet, P. Descouvemont, D. Baye, C. Leclercq-Willain, A. Coc, S. Barhoumi, P. Aguer, C. Rolfs, R. Kunz, J. W. Hammer, A. Mayer, T. Paradellis, S. Kossionides, C. Chronidou, K. Spyrou, S. degl’Innocenti, G. Fiorentini, B. Ricci, S. Zavatarelli, C. Providencia, H. Wolters, J. Soares, C. Grama, J. Rahighi, A. Shotter, and M. Laméhi Rachti, *Nucl. Phys. A* **656**, 3 (1999).
- [106] G. M. Fuller, W. A. Fowler, and M. J. Newman, *ApJ* **293**, 1 (1985).
- [107] T. Oda, M. Hino, K. Muto, M. Takahara, and K. Sato, *Atomic Data and Nuclear Data Tables* **56**, 231 (1994).
- [108] K. Langanke and G. Martínez-Pinedo, *Nuclear Physics A* **673**, 481 (2000), [nucl-th/0001018](#).
- [109] A. I. Chugunov, H. E. Dewitt, and D. G. Yakovlev, *PRD* **76**, 025028 (2007), [arXiv:0707.3500](#).
- [110] N. Itoh, H. Hayashi, A. Nishikawa, and Y. Kohyama, *ApJS* **102**, 411 (1996).
- [111] E. Anders and N. Grevesse, *Geochim. Cosmochim. Acta* **53**, 197 (1989).
- [112] S. Agostinelli et al. (GEANT4), *Nucl. Instrum. Meth. A* **506**, 250 (2003).
- [113] A. K. Harding and A. G. Muslimov, *The Astrophysical Journal* **743**, 181 (2011).
- [114] J. Cortés and L. Sironi, *ApJ* **933**, 140 (2022), [arXiv:2203.00023 \[astro-ph.HE\]](#).
- [115] J. Cortés and L. Sironi, *MNRAS* **534**, 2551 (2024), [arXiv:2404.03700 \[astro-ph.HE\]](#).

# Supplemental: Irradiated Pulsar Planets and Companions as 511 keV Sources

Zachary Metzler,<sup>1,2,3</sup> and Zorawar Wadiasingh,<sup>1,2,3</sup>

<sup>1</sup>University of Maryland, College Park

<sup>2</sup>NASA Goddard Space Flight Center

<sup>3</sup>Center for Research and Exploration in Space Science & Technology II

(Dated: March 14, 2025)

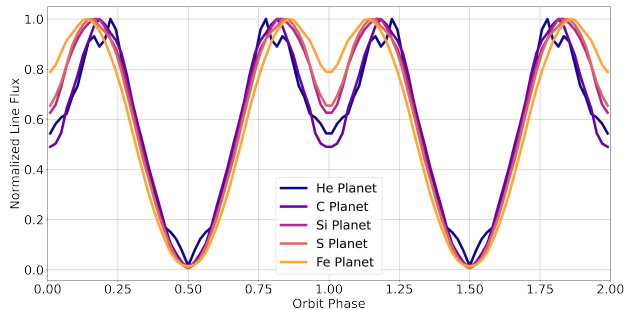


FIG. S1. The normalized 511 keV flux as a function of orbit for 5 planet models at  $i = 90^\circ$ .

*Composition Dependence of Pulse Shape* The orbital phase dependence of the 511 keV emission correlates with the atomic number,  $Z$ , of the planetary models. Figure S1 shows  $\hat{n}_{511}(\phi, i = \pi/2)$ , normalized such that the peak is set to 1, and only for the fluxes from the five planet models. The pulse shapes feature a double peak near when the MSP eclipses the planet, and the depth of the double peak with respect to the overall maximum flux decreases with increasing  $Z$ . Figure S2 shows that the depth of the double peak also correlates with the 511 keV production efficiency,  $\epsilon$ , which is expected given that Table I shows  $\epsilon$  increasing with  $Z$ .

The origin of the double peak feature comes from the fact that Coulomb losses, Bremsstrahlung, and photon scattering cross sections all scale with  $Z$ , but pair production scales roughly with  $Z^2$ . For higher  $Z$  materials, the electron positron pairs and subsequently the 511 keV photons are produced within fewer radiation lengths of the companions surface for higher  $Z$  materials. This explains the overall increase in  $\epsilon$  with  $Z$ . Coupled with the fact that the incident primary photons are traveling parallel, it explains the double peak and its  $Z$  dependence. Let the MSP be at  $z = +\infty$ , then the particle showers are all going to be in the  $-z$  direction along the path of the primary photon. For a photon that interacts near the center of the face of the companion, the shower is furthest from the surface, but for a photon that interacts near the edge of the face of the companion, the shower is closer to the surface, because the surface curves to be parallel with the  $z$  axis at the edge of the face of the companion. Since the 511 keV photons are produced within fewer radiation lengths of the surface for high  $Z$  materials, the effect of

the curvature of the face of the companion is reduced, and this leads to a shallower double peak than for low  $Z$  companions.

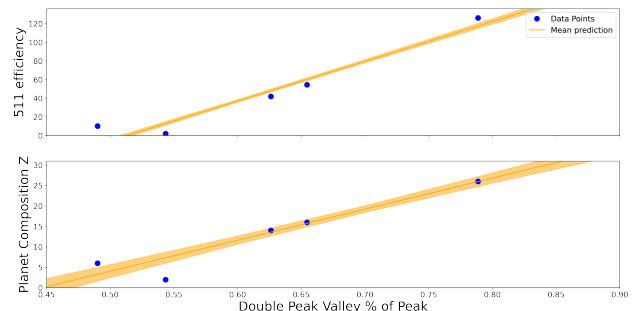


FIG. S2.  $\epsilon$  is shown as a function of  $\frac{\hat{n}_{511}(0, \frac{\pi}{2})}{\max(\hat{n}_{511}(\phi, \frac{\pi}{2}))}$  for each planetary model. All five models have the same density and radius with the only difference being the composition of the companion.

*Observable Characteristics* Observing the electron/positron annihilation line emission from MSP binary systems would provide a new window into the evolution of MSP systems, including constraining the NS mass and determining the composition of MSP binary companions. Suppose a nearby MSP's pulsed gamma ray emission is observed; one can measure the gamma ray luminosity from the MSP  $L_{\text{MSP}}$ , the spectrum  $\frac{dN}{dE}$ , and a binary mass function (Equation S1) from the orbital period and the peak radial velocity of the MSP,  $K_{\text{MSP}}$ . Equivalently, measuring the binary's GW strain with LISA can constrain  $M_c$ ,  $P_{\text{orb}}$ , and the inclination angle. Methods for accurately identifying the MSP binary from other galactic binaries with LISA data are beyond the scope of this work.

$$\frac{M_{\text{comp}}^3 \sin^3(i)}{M_{\text{tot}}^2} = \frac{P_{\text{orb}} K_{\text{MSP}}^3}{2\pi G} \quad (\text{S1})$$

More constraints can be placed with the additional measurements of the annihilation line flux, the flux profile over the duration of the orbit, and the Doppler shifts of the line throughout the orbit. The Doppler shifts constrain the radial velocity of the companion as Equation S2, which determines a second binary mass function in a similar manner to Equation S1.

$$\frac{\Delta E}{E} = \frac{c}{c - K_{\text{comp}}} \quad (\text{S2})$$

Without GW measurements, the 511 keV flux variation throughout the orbit constrains the inclination angle, where face-on inclination has a constant flux. Edge-on inclination has a prominent eclipse at the superior conjunction of the MSP. This variation is illustrated in Figure 5. From the inclination and the two mass functions or one mass function and the GW measurements, one can derive the NS and companion masses. With the masses, the semi-major axis,  $a$ , can be found with Equation S3.

$$G(M_{\text{NS}} + M_{\text{comp}}) = \left( \frac{2\pi}{P_{\text{orb}}} \right)^2 a^3 \quad (\text{S3})$$

If the inclination angle is shallow enough, the line flux variation throughout the orbit also constrains  $\epsilon$  by the depth of the gap between the double peak at the ecliptic. A shallower gap is correlated to more efficient production of escaped annihilation photons and to a higher-Z companion, as demonstrated with Figure S2. Further, if the inclination angle is small enough, then the form of  $f(\phi, i = \frac{\pi}{2})$  can be approximated to find  $\dot{N}_{511}$ . The solid angle of the companion can be found with Equation S4, where  $\dot{N}_{\text{MSP}}$  is the total rate of photons emitted by the MSP.

$$\Delta\Omega = 4\pi \frac{\dot{N}_{511}}{\epsilon \dot{N}_{\text{MSP}}} \quad (\text{S4})$$

Finally, the solid angle,  $\Delta\Omega$ , taken with the semi-major axis,  $a$ , determine the companion radius,  $R$ , as in Equation S5

$$\Delta\Omega = 2\pi [1 - \cos(\psi)] \quad , \quad \tan(\psi) = \frac{R}{a} \quad (\text{S5})$$

In this way, measurement of the flux of the 511 keV line combined with either pulsar timing or the binary's GW strain can constrain the composition and density of the companion in a MSP binary system.

*Other Possible Primary Radiation Channels* The main text focuses on  $L_{511,i}$ , which is the 511 keV back-splash emission due to incident GeV gamma rays from the MSP current sheet. We briefly consider the other four channels and address why they are not included in the main analysis.

The second channel,  $L_{511,ii}$ , is the effect of relativistic  $e^+e^-$  pairs produced at the polar cap in the MSP and advected out into the wind. To model this, we replaced the gamma ray flux from the simulation with incident  $e^+e^-$  pairs with a luminosity,  $L_{e^+e^-,pc} = 10^{34}$  erg/s, and

a spectrum that follows that of a MSP with  $P_{\text{rot}} = 2$  ms, 0 degree offset, and  $B = 2 \times 10^9$  G from [S113]. For this simulation, we injected 10,000  $e^-e^+$  pairs with the Fe planet model and tracked the escaping gamma rays.

The third channel,  $L_{511,iii}$ , is the effect of ultra-relativistic 10-100 TeV  $e^-e^+$  pairs. Due to limitations with the simulation, simulating a statistically significant number of 100 TeV particles would take an unreasonable amount of time. Therefore, we instead simulated 10,000 pairs each of monochromatic 1, 10, and 100 GeV particles with the Fe planet model with  $L_{e^+e^-,\text{TeV}} = 10^{34}$  erg/s. Then, we project  $L_{511}$  from these lower energy particles to 10 TeV to get a rough estimate of  $L_{511}$ .

The fourth channel,  $L_{511,iv}$ , is the effect of protons accelerated to GeV energies. Our simulations neglected nuclear effects, including activation of the companion crust by charged particle bombardment. As such, it would have been unreasonable to include proton bombardment without nuclear interactions. A future study will reconsider the impact of nuclear interactions on the 511 keV emission as well as the presence of other activation lines.

The fifth channel,  $L_{511,v}$ , is the result of shock formation between the MSP and the companion for BW and RB systems. The shock produces a power law with exponential cutoff spectrum with unknown cutoff energy between  $\gtrsim 100$  keV and  $\sim 150$  MeV  $\sim m_e c^2 / \alpha_f$  [e.g., S78, S79, S114, S115]. For this simulation, we produce 10,000 photons on half of the sky from the perspective of the companion as opposed to a far field point source. The spectrum used is the same as in Equation 2 with  $E_0 = 150$  MeV,  $\Gamma = 1.67$ ,  $d = 0.1$ , and  $b = 3$ . This simulation assumes a gamma ray luminosity of  $L_{\text{shock}} = 10^{32}$  erg/s, and uses the Fe planet model. This assumption represents the upper limit of  $L_{511,iv}$ , because a lower cutoff energy potentially drastically reduces the line production efficiency.

$L_{511}$  is presented in Table S1 for all of the considered production channels along with the steps used to reach  $L_{511,iii}$ . Only  $L_{511,i}$  was presented in the main text, because  $L_{511,ii}$  is negligible,  $L_{511,iii}$  requires projecting the 511 efficiency over two orders of magnitude, this analysis neglected nuclear interactions for  $L_{511,iv}$ , and the cutoff energy of the primary gamma ray spectrum for  $L_{511,iv}$  is unconstrained by observations. Taking each of these simulations at face value suggests that  $L_{511}$  could be substantially larger than  $L_{511,i}$ , but the uncertainties on companion composition and size represent larger uncertainties than those from neglecting  $L_{511,ii,iii,iv,v}$  in the main text.

Channel	$L_{511}$ [erg/s]
Primary GeV $\gamma$ -rays, $L_{511,i}$	$10^{25.5} L_{\text{MSP},34}$
*Primary $e^-e^+$ Pairs, $L_{511,ii}$	$10^{23.4} L_{ee,34}$
Mono. 1 GeV $e^+e^-$ Pairs	$10^{22.5} L_{34}$
Mono. 10 GeV $e^+e^-$ Pairs	$10^{23.2} L_{34}$
Mono. 100 GeV $e^+e^-$ Pairs	$10^{23.9} L_{34}$
Mono. 1 TeV $e^+e^-$ Pairs (proj.)	$10^{24.6} L_{34}$
Mono. 10 TeV $e^+e^-$ Pairs (proj.), $L_{511,iii}$	$10^{25.3} L_{34}$
**Shock MeV $\gamma$ -rays, $L_{511,v}$	$10^{25.7} L_{\text{Shock},32}$

TABLE S1. For the ideal Fe planet model, we calculate  $L_{511}$  for each of the primary radiation channels from Equation 2. \* Solid Blue line Fig 10 of [S113]. \*\* Power law with exponential cutoff as in Equation A.7 with  $E_0 = 150$  MeV,  $\Gamma = 1.67$ ,  $d = 0.1$ , and  $b = 3$ .



Name	3PC	$L_{\text{MSP}}$	Mass	$P_{\text{orb}}$	Separation	Distance	Radius	Average Density	Peak Flux
Units	–	ergs/s	$M_{\odot}$	s	cm	pc	cm	$\text{g}/\text{cm}^3$	$\text{ph}/\text{cm}^2/\text{s}$
J1737-0811	No	$8.6 \times 10^{32}$	0.076	$6.9 \times 10^6$	$6.6 \times 10^{12}$	206	$2 \times 10^{10}$	10	$1.3 \times 10^{-13}$
							$1 \times 10^{10}$	30	$6.3 \times 10^{-14}$
							$6 \times 10^8$	$1.7 \times 10^5$	$2.0 \times 10^{-16}$
J1502-6752	No	$1.3 \times 10^{32}$	0.025	$2.1 \times 10^5$	$6.5 \times 10^{11}$	7866	$1 \times 10^{10}$	10	$6.7 \times 10^{-16}$
							$7 \times 10^9$	30	$3.2 \times 10^{-16}$
							$6 \times 10^8$	$5.6 \times 10^4$	$2.1 \times 10^{-18}$
J1300+1240	No	$3.8 \times 10^{33}$	5.6e-08	$2.2 \times 10^6$	$3.0 \times 10^{12}$	709	$1 \times 10^8$	10	$1.9 \times 10^{-17}$
							$1 \times 10^8$	30	$9.0 \times 10^{-18}$
							$6 \times 10^8$	0	$3.5 \times 10^{-16}$

TABLE S2. The line flux estimates for the UL systems listed in the ATNF Pulsar Catalogue. We list three different assumptions for the radius and density of the companions 1)  $10 \text{ g}/\text{cm}^3$ , 2)  $30 \text{ g}/\text{cm}^3$ , 3) Earth radius. The values for companion mass and distance are taken from the ATNF Pulsar Catalogue [S80]. The companion mass used here is the median mass according to the ATNF Pulsar Catalogue. The separation is calculated from the orbit period listed in the ATNF Pulsar Catalogue.

Name	3PC	$L_{\text{MSP}}$	Mass	$P_{\text{orb}}$	Separation	Distance	Radius	Average Density	Peak Flux
Units	–	ergs/s	$M_{\odot}$	s	cm	pc	cm	$\text{g}/\text{cm}^3$	$\text{ph}/\text{cm}^2/\text{s}$
J1757-5322	No	$3.0 \times 10^{32}$	0.67	$3.9 \times 10^4$	$2.3 \times 10^{11}$	945	$7 \times 10^8$	$9.3 \times 10^5$	$2.7 \times 10^{-16}$
J1802-2124	No	$2.8 \times 10^{32}$	0.98	$6.0 \times 10^4$	$3.2 \times 10^{11}$	800	$7 \times 10^8$	$1.4 \times 10^6$	$1.9 \times 10^{-16}$
J2222-0137	No	$1.3 \times 10^{32}$	1.4	$2.1 \times 10^5$	$7.7 \times 10^{11}$	268	$7 \times 10^8$	$1.9 \times 10^6$	$1.3 \times 10^{-16}$
J1614-2230	Yes	$2.4 \times 10^{33}$	0.47	$7.5 \times 10^5$	$1.6 \times 10^{12}$	700	$7 \times 10^8$	$6.6 \times 10^5$	$8.3 \times 10^{-17}$
J1952+2630	No	$3.8 \times 10^{33}$	1.1	$3.4 \times 10^4$	$2.2 \times 10^{11}$	10031	$7 \times 10^8$	$1.6 \times 10^6$	$3.3 \times 10^{-17}$
J1658+3630	No	$2.5 \times 10^{31}$	1.1	$2.6 \times 10^5$	$8.6 \times 10^{11}$	224	$7 \times 10^8$	$1.5 \times 10^6$	$3.0 \times 10^{-17}$
J1525-5545	No	$7.1 \times 10^{32}$	0.99	$8.6 \times 10^4$	$4.1 \times 10^{11}$	3140	$7 \times 10^8$	$1.4 \times 10^6$	$1.9 \times 10^{-17}$
J1439-5501	No	$4.8 \times 10^{31}$	1.4	$1.8 \times 10^5$	$7.0 \times 10^{11}$	655	$7 \times 10^8$	$1.9 \times 10^6$	$9.7 \times 10^{-18}$
J1933-6211	No	$6.9 \times 10^{32}$	0.38	$1.1 \times 10^6$	$2.1 \times 10^{12}$	1000	$7 \times 10^8$	$5.3 \times 10^5$	$7.1 \times 10^{-18}$
J1435-6100	No	$2.4 \times 10^{32}$	1.1	$1.2 \times 10^5$	$5.0 \times 10^{11}$	2816	$7 \times 10^8$	$1.5 \times 10^6$	$5.1 \times 10^{-18}$
J1045-0436	No	$4.5 \times 10^{31}$	0.98	$8.9 \times 10^5$	$1.9 \times 10^{12}$	329	$7 \times 10^8$	$1.4 \times 10^6$	$4.8 \times 10^{-18}$
J2053+4650	No	$6.8 \times 10^{32}$	1.0	$2.1 \times 10^5$	$7.4 \times 10^{11}$	3810	$7 \times 10^8$	$1.4 \times 10^6$	$3.7 \times 10^{-18}$
J2145-0750	No	$5.7 \times 10^{31}$	0.5	$5.9 \times 10^5$	$1.4 \times 10^{12}$	625	$7 \times 10^8$	$7.0 \times 10^5$	$3.3 \times 10^{-18}$
J1022+1001	No	$7.7 \times 10^{31}$	0.85	$6.7 \times 10^5$	$1.6 \times 10^{12}$	725	$7 \times 10^8$	$1.2 \times 10^6$	$2.5 \times 10^{-18}$
J0900-3144	No	$2.8 \times 10^{32}$	0.42	$1.6 \times 10^6$	$2.7 \times 10^{12}$	900	$7 \times 10^8$	$5.9 \times 10^5$	$2.1 \times 10^{-18}$
J0824+0028	No	$1.2 \times 10^{33}$	0.4	$2.0 \times 10^6$	$3.1 \times 10^{12}$	1689	$7 \times 10^8$	$5.6 \times 10^5$	$2.0 \times 10^{-18}$
J1949+3106	No	$3.3 \times 10^{32}$	0.97	$1.7 \times 10^5$	$6.3 \times 10^{11}$	7468	$7 \times 10^8$	$1.3 \times 10^6$	$6.3 \times 10^{-19}$
J0721-2038	No	$9.3 \times 10^{31}$	0.55	$4.7 \times 10^5$	$1.2 \times 10^{12}$	2680	$7 \times 10^8$	$7.6 \times 10^5$	$3.9 \times 10^{-19}$
J1101-6424	No	$1.1 \times 10^{32}$	0.57	$8.3 \times 10^5$	$1.7 \times 10^{12}$	2175	$7 \times 10^8$	$7.9 \times 10^5$	$3.2 \times 10^{-19}$
J1943+2210	No	$5.3 \times 10^{32}$	0.33	$7.2 \times 10^5$	$1.5 \times 10^{12}$	6773	$7 \times 10^8$	$4.6 \times 10^5$	$2.2 \times 10^{-19}$
J1337-6423	No	$2.3 \times 10^{32}$	0.95	$4.1 \times 10^5$	$1.2 \times 10^{12}$	5951	$7 \times 10^8$	$1.3 \times 10^6$	$2.1 \times 10^{-19}$
J1938+6604	No	$1.4 \times 10^{31}$	1.0	$2.1 \times 10^5$	$7.5 \times 10^{11}$	3379	$7 \times 10^8$	$1.4 \times 10^6$	$9.4 \times 10^{-20}$
J1603-7202	No	$3.8 \times 10^{31}$	0.34	$5.5 \times 10^5$	$1.3 \times 10^{12}$	3700	$7 \times 10^8$	$4.7 \times 10^5$	$7.4 \times 10^{-20}$
J1933+1726	No	$3.9 \times 10^{31}$	0.94	$4.5 \times 10^5$	$1.2 \times 10^{12}$	4072	$7 \times 10^8$	$1.3 \times 10^6$	$6.9 \times 10^{-20}$
J1755-3716	No	$1.2 \times 10^{32}$	0.35	$9.9 \times 10^5$	$1.9 \times 10^{12}$	8178	$7 \times 10^8$	$4.9 \times 10^5$	$2.1 \times 10^{-20}$

TABLE S3. The line flux estimates for C WD-MSP systems in the ATNF Pulsar Catalogue. The values for companion mass and distance are taken from the ATNF Pulsar Catalogue [S80]. The companion mass used here is the median mass according to the ATNF Pulsar Catalogue. The separation is calculated from the orbit period listed in the ATNF Pulsar Catalogue. The radius is the lesser value of either the size of the Roche lobe or the radius of the model used in the Methods section. The density column is the average density assuming a homogeneous sphere with the companion mass and radius.

Name	3PC	$L_{\text{MSP}}$	Mass	$P_{\text{orb}}$	Separation	Distance	Radius	Average Density	Model	Peak Flux
Units	–	ergs/s	$M_{\odot}$	s	cm	pc	cm	$\text{g}/\text{cm}^3$	–	$\text{ph}/\text{cm}^2/\text{s}$
J2339-0533	Yes	$4.6 \times 10^{33}$	0.3	$1.7 \times 10^4$	$1.2 \times 10^{11}$	1100	$2 \times 10^{10}$	18	0.3 MS	$1.2 \times 10^{-12}$
J2215+5135	Yes	$1.5 \times 10^{34}$	0.24	$1.5 \times 10^4$	$1.1 \times 10^{11}$	2773	$2 \times 10^{10}$	15	0.3 MS	$6.8 \times 10^{-13}$
J1431-4715	Yes	$1.4 \times 10^{34}$	0.14	$3.9 \times 10^4$	$2.1 \times 10^{11}$	1562	$8 \times 10^9$	$1.2 \times 10^2$	0.1 MS	$9.7 \times 10^{-14}$
J1816+4510	Yes	$1.0 \times 10^{34}$	0.18	$3.1 \times 10^4$	$1.8 \times 10^{11}$	4356	$8 \times 10^9$	$1.5 \times 10^2$	0.1 MS	$1.3 \times 10^{-14}$

TABLE S4. The line flux estimates for MS star-MSP systems in the ATNF Pulsar Catalogue. The values for companion mass and distance are taken from the ATNF Pulsar Catalogue [S80]. The companion mass used here is the median mass according to the ATNF Pulsar Catalogue. The separation is calculated from the orbit period listed in the ATNF Pulsar Catalogue. The radius is the lesser value of either the size of the Roche lobe or the radius of the model used in the Methods section. The density column is the average density assuming a homogeneous sphere with the companion mass and radius. The model column lists which model from the Methods section is used.

Name	3PC	$L_{\text{MSP}}$	Mass	$P_{\text{orb}}$	Separation	Distance	Radius	Average Density	Peak Flux
Units	–	ergs/s	$M_{\odot}$	s	cm	pc	cm	$\text{g}/\text{cm}^3$	$\text{ph}/\text{cm}^2/\text{s}$
J1720-0533	No	$1.8 \times 10^{33}$	0.034	$1.1 \times 10^4$	$9.1 \times 10^{10}$	191	$1 \times 10^{10}$	10	$9.4 \times 10^{-10}$
							$8 \times 10^9$	30	$4.7 \times 10^{-10}$
							$6 \times 10^8$	$7.5 \times 10^4$	$2.6 \times 10^{-12}$
J1959+2048	Yes	$3.2 \times 10^{34}$	0.025	$3.3 \times 10^4$	$1.9 \times 10^{11}$	1400	$1 \times 10^{10}$	10	$6.3 \times 10^{-11}$
							$7 \times 10^9$	30	$3.0 \times 10^{-11}$
							$6 \times 10^8$	$5.5 \times 10^4$	$2.0 \times 10^{-13}$
J2241-5236	Yes	$5.2 \times 10^{33}$	0.014	$1.3 \times 10^4$	$9.7 \times 10^{10}$	1042	$9 \times 10^9$	10	$4.5 \times 10^{-11}$
							$6 \times 10^9$	30	$2.1 \times 10^{-11}$
							$6 \times 10^8$	$3.0 \times 10^4$	$2.2 \times 10^{-13}$
J1701-3006F	No	$1.5 \times 10^{35}$	0.024	$1.8 \times 10^4$	$1.2 \times 10^{11}$	6410	$1 \times 10^{10}$	10	$3.0 \times 10^{-11}$
							$7 \times 10^9$	30	$1.5 \times 10^{-11}$
							$6 \times 10^8$	$5.3 \times 10^4$	$1.0 \times 10^{-13}$
J1701-3006E	No	$7.2 \times 10^{34}$	0.035	$1.4 \times 10^4$	$1.0 \times 10^{11}$	6410	$1 \times 10^{10}$	10	$2.7 \times 10^{-11}$
							$8 \times 10^9$	30	$1.3 \times 10^{-11}$
							$6 \times 10^8$	$7.8 \times 10^4$	$7.0 \times 10^{-14}$
J2214+3000	Yes	$3.8 \times 10^{33}$	0.015	$3.6 \times 10^4$	$2.0 \times 10^{11}$	600	$9 \times 10^9$	10	$2.7 \times 10^{-11}$
							$6 \times 10^9$	30	$1.3 \times 10^{-11}$
							$6 \times 10^8$	$3.4 \times 10^4$	$1.2 \times 10^{-13}$
J0251+2606	Yes	$3.6 \times 10^{33}$	0.028	$1.7 \times 10^4$	$1.2 \times 10^{11}$	1170	$1 \times 10^{10}$	10	$2.6 \times 10^{-11}$
							$8 \times 10^9$	30	$1.2 \times 10^{-11}$
							$6 \times 10^8$	$6.2 \times 10^4$	$7.7 \times 10^{-14}$
J0024-7204R	No	$2.8 \times 10^{34}$	0.03	$5.7 \times 10^3$	$5.8 \times 10^{10}$	4520	$7 \times 10^9$	41	$2.4 \times 10^{-11}$
							$7 \times 10^9$	41	$2.4 \times 10^{-11}$
							$6 \times 10^8$	$6.6 \times 10^4$	$1.7 \times 10^{-13}$
J1641+8049	Yes	$8.6 \times 10^{33}$	0.047	$7.9 \times 10^3$	$7.1 \times 10^{10}$	3035	$1 \times 10^{10}$	22	$2.1 \times 10^{-11}$
							$9 \times 10^9$	30	$1.7 \times 10^{-11}$
							$6 \times 10^8$	$1.0 \times 10^5$	$7.7 \times 10^{-14}$
J2234+0944	Yes	$3.3 \times 10^{33}$	0.018	$3.6 \times 10^4$	$2.0 \times 10^{11}$	714	$9 \times 10^9$	10	$1.8 \times 10^{-11}$
							$7 \times 10^9$	30	$8.5 \times 10^{-12}$
							$6 \times 10^8$	$3.9 \times 10^4$	$7.1 \times 10^{-14}$
J0636+5128	Yes	$1.2 \times 10^{33}$	0.0079	$5.8 \times 10^3$	$5.8 \times 10^{10}$	714	$5 \times 10^9$	39	$1.7 \times 10^{-11}$
							$5 \times 10^9$	39	$1.7 \times 10^{-11}$
							$6 \times 10^8$	$1.8 \times 10^4$	$2.9 \times 10^{-13}$
J1446-4701	Yes	$7.3 \times 10^{33}$	0.022	$2.4 \times 10^4$	$1.5 \times 10^{11}$	1569	$1 \times 10^{10}$	10	$1.6 \times 10^{-11}$
							$7 \times 10^9$	30	$7.8 \times 10^{-12}$
							$6 \times 10^8$	$4.9 \times 10^4$	$5.6 \times 10^{-14}$
J1555-2908	Yes	$6.2 \times 10^{34}$	0.059	$2.0 \times 10^4$	$1.3 \times 10^{11}$	7559	$1 \times 10^{10}$	10	$1.4 \times 10^{-11}$
							$1 \times 10^{10}$	30	$6.8 \times 10^{-12}$
							$6 \times 10^8$	$1.3 \times 10^5$	$2.5 \times 10^{-14}$
J0023+0923	Yes	$3.2 \times 10^{33}$	0.019	$1.2 \times 10^4$	$9.4 \times 10^{10}$	1818	$1 \times 10^{10}$	10	$1.2 \times 10^{-11}$
							$7 \times 10^9$	30	$5.7 \times 10^{-12}$
							$6 \times 10^8$	$4.2 \times 10^4$	$4.6 \times 10^{-14}$
J1221-0633	Yes	$5.7 \times 10^{33}$	0.015	$3.3 \times 10^4$	$1.9 \times 10^{11}$	1251	$9 \times 10^9$	10	$1.0 \times 10^{-11}$
							$6 \times 10^9$	30	$4.8 \times 10^{-12}$
							$6 \times 10^8$	$3.4 \times 10^4$	$4.5 \times 10^{-14}$
J1957+2516	No	$3.5 \times 10^{33}$	0.11	$2.1 \times 10^4$	$1.4 \times 10^{11}$	2659	$2 \times 10^{10}$	10	$9.3 \times 10^{-12}$
							$1 \times 10^{10}$	30	$4.5 \times 10^{-12}$
							$6 \times 10^8$	$2.5 \times 10^5$	$1.1 \times 10^{-14}$
J2051-0827	Yes	$1.1 \times 10^{33}$	0.031	$8.6 \times 10^3$	$7.5 \times 10^{10}$	1469	$9 \times 10^9$	18	$9.0 \times 10^{-12}$
							$8 \times 10^9$	30	$6.5 \times 10^{-12}$
							$6 \times 10^8$	$6.8 \times 10^4$	$3.8 \times 10^{-14}$
J1719-1438	No	$3.3 \times 10^{32}$	0.0013	$7.8 \times 10^3$	$7.1 \times 10^{10}$	336	$3 \times 10^9$	20	$6.7 \times 10^{-12}$
							$3 \times 10^9$	30	$5.2 \times 10^{-12}$
							$6 \times 10^8$	$2.9 \times 10^3$	$2.5 \times 10^{-13}$
J1630+3550	No	$4.9 \times 10^{33}$	0.011	$2.7 \times 10^4$	$1.6 \times 10^{11}$	1568	$8 \times 10^9$	10	$5.9 \times 10^{-12}$
							$6 \times 10^9$	30	$2.8 \times 10^{-12}$
							$6 \times 10^8$	$2.5 \times 10^4$	$3.2 \times 10^{-14}$

Name	3PC	$L_{\text{MSP}}$	Mass	$P_{\text{orb}}$	Separation	Distance	Radius	Average Density	Peak Flux
Units	–	ergs/s	$M_{\odot}$	s	cm	pc	cm	$\text{g}/\text{cm}^3$	$\text{ph}/\text{cm}^2/\text{s}$
J1805+0615	Yes	$1.9 \times 10^{34}$	0.027	$2.9 \times 10^4$	$1.7 \times 10^{11}$	3885	$1 \times 10^{10}$	10	$5.8 \times 10^{-12}$
							$8 \times 10^9$	30	$2.8 \times 10^{-12}$
							$6 \times 10^8$	$5.9 \times 10^4$	$1.8 \times 10^{-14}$
J0610-2100	Yes	$1.7 \times 10^{33}$	0.025	$2.5 \times 10^4$	$1.5 \times 10^{11}$	1389	$1 \times 10^{10}$	10	$4.9 \times 10^{-12}$
							$7 \times 10^9$	30	$2.4 \times 10^{-12}$
							$6 \times 10^8$	$5.5 \times 10^4$	$1.6 \times 10^{-14}$
J1731-1847	No	$1.6 \times 10^{34}$	0.039	$2.7 \times 10^4$	$1.6 \times 10^{11}$	4782	$1 \times 10^{10}$	10	$4.6 \times 10^{-12}$
							$8 \times 10^9$	30	$2.2 \times 10^{-12}$
							$6 \times 10^8$	$8.5 \times 10^4$	$1.1 \times 10^{-14}$
J1544+4937	Yes	$2.2 \times 10^{33}$	0.02	$1.0 \times 10^4$	$8.6 \times 10^{10}$	2990	$9 \times 10^9$	12	$3.3 \times 10^{-12}$
							$7 \times 10^9$	30	$1.8 \times 10^{-12}$
							$6 \times 10^8$	$4.3 \times 10^4$	$1.4 \times 10^{-14}$
J1641+3627E	No	$9.0 \times 10^{33}$	0.023	$9.7 \times 10^3$	$8.2 \times 10^{10}$	7500	$9 \times 10^9$	14	$2.4 \times 10^{-12}$
							$7 \times 10^9$	30	$1.4 \times 10^{-12}$
							$6 \times 10^8$	$5.1 \times 10^4$	$1.0 \times 10^{-14}$
J1745+1017	Yes	$1.2 \times 10^{33}$	0.016	$6.3 \times 10^4$	$2.8 \times 10^{11}$	1214	$9 \times 10^9$	10	$9.5 \times 10^{-13}$
							$6 \times 10^9$	30	$4.5 \times 10^{-13}$
							$6 \times 10^8$	$3.5 \times 10^4$	$4.1 \times 10^{-15}$
J2055+3829	No	$8.7 \times 10^{32}$	0.026	$1.1 \times 10^4$	$9.0 \times 10^{10}$	4588	$1 \times 10^{10}$	11	$6.5 \times 10^{-13}$
							$7 \times 10^9$	30	$3.3 \times 10^{-13}$
							$6 \times 10^8$	$5.7 \times 10^4$	$2.2 \times 10^{-15}$
J1836-2354A	No	$4.8 \times 10^{32}$	0.02	$1.8 \times 10^4$	$1.2 \times 10^{11}$	3300	$1 \times 10^{10}$	10	$3.4 \times 10^{-13}$
							$7 \times 10^9$	30	$1.6 \times 10^{-13}$
							$6 \times 10^8$	$4.3 \times 10^4$	$1.3 \times 10^{-15}$
J1850+0242	No	$1.4 \times 10^{34}$	0.083	$6.4 \times 10^4$	$2.9 \times 10^{11}$	12311	$2 \times 10^{10}$	10	$3.3 \times 10^{-13}$
							$1 \times 10^{10}$	30	$1.6 \times 10^{-13}$
							$6 \times 10^8$	$1.8 \times 10^5$	$4.8 \times 10^{-16}$
J1317-0157	No	$1.8 \times 10^{33}$	0.02	$7.7 \times 10^3$	$7.0 \times 10^{10}$	25000	$8 \times 10^9$	22	$3.8 \times 10^{-14}$
							$7 \times 10^9$	30	$3.2 \times 10^{-14}$
							$6 \times 10^8$	$4.5 \times 10^4$	$2.4 \times 10^{-16}$
J2322-2650	No	$1.1 \times 10^{32}$	0.00085	$2.8 \times 10^4$	$1.6 \times 10^{11}$	2000	$3 \times 10^9$	10	$1.4 \times 10^{-14}$
							$2 \times 10^9$	30	$6.9 \times 10^{-15}$
							$6 \times 10^8$	$1.9 \times 10^3$	$4.3 \times 10^{-16}$

TABLE S5: The line flux estimates for the BW systems listed in the ATNF Pulsar Catalogue. We list three different assumptions for the radius and density of the companions 1)  $10 \text{ g}/\text{cm}^3$ , 2)  $30 \text{ g}/\text{cm}^3$ , 3) Earth radius. The values for companion mass and distance are taken from the ATNF Pulsar Catalogue [S80]. The companion mass used here is the median mass according to the ATNF Pulsar Catalogue. The separation is calculated from the orbit period listed in the ATNF Pulsar Catalogue.

Name	3PC	$L_{\text{MSP}}$	Mass	$P_{\text{orb}}$	Separation	Distance	Radius	Average Density	Peak Flux
Units	–	ergs/s	$M_{\odot}$	s	cm	pc	cm	$\text{g}/\text{cm}^3$	$\text{ph}/\text{cm}^2/\text{s}$
J0751+1807	Yes	$1.5 \times 10^{33}$	0.15	$2.3 \times 10^4$	$1.5 \times 10^{11}$	600	$2 \times 10^{10}$	9	$1.5 \times 10^{-12}$
J0437-4715	Yes	$2.4 \times 10^{33}$	0.16	$5.0 \times 10^5$	$1.2 \times 10^{12}$	157	$2 \times 10^{10}$	10	$5.8 \times 10^{-13}$
J1231-1411	Yes	$3.6 \times 10^{33}$	0.22	$1.6 \times 10^5$	$5.5 \times 10^{11}$	420	$2 \times 10^{10}$	13	$5.3 \times 10^{-13}$
J0742+4110	No	$1.7 \times 10^{33}$	0.067	$1.2 \times 10^5$	$4.4 \times 10^{11}$	523	$2 \times 10^{10}$	4	$2.6 \times 10^{-13}$
J0621+2514	Yes	$9.7 \times 10^{33}$	0.17	$1.1 \times 10^5$	$4.2 \times 10^{11}$	1641	$2 \times 10^{10}$	10	$1.6 \times 10^{-13}$
J0613-0200	Yes	$2.6 \times 10^{33}$	0.15	$1.0 \times 10^5$	$4.1 \times 10^{11}$	950	$2 \times 10^{10}$	9	$1.4 \times 10^{-13}$
J0337+1715	No	$6.8 \times 10^{33}$	0.14	$1.4 \times 10^5$	$5.0 \times 10^{11}$	1300	$2 \times 10^{10}$	8	$1.3 \times 10^{-13}$
J1902-5105	Yes	$1.4 \times 10^{34}$	0.19	$1.7 \times 10^5$	$5.8 \times 10^{11}$	1645	$2 \times 10^{10}$	11	$1.2 \times 10^{-13}$
J0218+4232	Yes	$4.9 \times 10^{34}$	0.2	$1.8 \times 10^5$	$5.8 \times 10^{11}$	3150	$2 \times 10^{10}$	12	$1.2 \times 10^{-13}$
J1909-3744	Yes	$4.3 \times 10^{33}$	0.23	$1.3 \times 10^5$	$4.9 \times 10^{11}$	1140	$2 \times 10^{10}$	14	$1.1 \times 10^{-13}$
J0034-0534	Yes	$5.9 \times 10^{33}$	0.16	$1.4 \times 10^5$	$4.9 \times 10^{11}$	1348	$2 \times 10^{10}$	10	$1.1 \times 10^{-13}$
J1514-4946	Yes	$3.2 \times 10^{33}$	0.2	$1.7 \times 10^5$	$5.6 \times 10^{11}$	908	$2 \times 10^{10}$	12	$9.8 \times 10^{-14}$
J0024-7204U	No	$9.2 \times 10^{33}$	0.14	$3.7 \times 10^4$	$2.0 \times 10^{11}$	4520	$2 \times 10^{10}$	9	$8.5 \times 10^{-14}$
J1738+0333	No	$9.5 \times 10^{32}$	0.1	$3.1 \times 10^4$	$1.8 \times 10^{11}$	1695	$2 \times 10^{10}$	6	$8.2 \times 10^{-14}$
J1400-1431	Yes	$1.9 \times 10^{33}$	0.31	$8.2 \times 10^5$	$1.7 \times 10^{12}$	278	$2 \times 10^{10}$	19	$7.3 \times 10^{-14}$
J0101-6422	Yes	$2.4 \times 10^{33}$	0.18	$1.5 \times 10^5$	$5.3 \times 10^{11}$	1001	$2 \times 10^{10}$	11	$6.7 \times 10^{-14}$
J2043+1711	Yes	$3.1 \times 10^{33}$	0.2	$1.3 \times 10^5$	$4.7 \times 10^{11}$	1389	$2 \times 10^{10}$	12	$5.7 \times 10^{-14}$
J2006+0148	Yes	$2.6 \times 10^{33}$	0.18	$5.6 \times 10^4$	$2.7 \times 10^{11}$	2437	$2 \times 10^{10}$	10	$4.7 \times 10^{-14}$
J1543-5149	Yes	$1.5 \times 10^{34}$	0.26	$7.0 \times 10^5$	$1.5 \times 10^{12}$	1149	$2 \times 10^{10}$	16	$4.1 \times 10^{-14}$
J1625-0021	Yes	$7.4 \times 10^{33}$	0.19	$6.4 \times 10^5$	$1.4 \times 10^{12}$	951	$2 \times 10^{10}$	11	$3.5 \times 10^{-14}$
J1911-1114	No	$2.3 \times 10^{33}$	0.14	$2.3 \times 10^5$	$7.0 \times 10^{11}$	1069	$2 \times 10^{10}$	8	$3.3 \times 10^{-14}$
J1701-3006D	No	$2.5 \times 10^{34}$	0.14	$9.7 \times 10^4$	$3.9 \times 10^{11}$	6410	$2 \times 10^{10}$	8	$3.2 \times 10^{-14}$
J1835-3259B	Yes	$5.6 \times 10^{34}$	0.2	$1.0 \times 10^5$	$4.1 \times 10^{11}$	9460	$2 \times 10^{10}$	12	$3.0 \times 10^{-14}$
J2017+0603	Yes	$2.6 \times 10^{33}$	0.21	$1.9 \times 10^5$	$6.1 \times 10^{11}$	1399	$2 \times 10^{10}$	12	$2.8 \times 10^{-14}$
J1045-4509	No	$3.3 \times 10^{32}$	0.19	$3.5 \times 10^5$	$9.3 \times 10^{11}$	340	$2 \times 10^{10}$	11	$2.7 \times 10^{-14}$
J0740+6620	Yes	$4.0 \times 10^{33}$	0.22	$4.1 \times 10^5$	$1.0 \times 10^{12}$	1150	$2 \times 10^{10}$	13	$2.3 \times 10^{-14}$
J1745-0952	No	$1.0 \times 10^{32}$	0.13	$4.3 \times 10^5$	$1.0 \times 10^{12}$	226	$2 \times 10^{10}$	7	$1.5 \times 10^{-14}$
J0024-7204T	No	$5.3 \times 10^{33}$	0.2	$9.7 \times 10^4$	$3.9 \times 10^{11}$	4520	$2 \times 10^{10}$	12	$1.3 \times 10^{-14}$
J0605+3757	Yes	$1.8 \times 10^{33}$	0.21	$4.8 \times 10^6$	$5.3 \times 10^{12}$	215	$2 \times 10^{10}$	12	$1.1 \times 10^{-14}$
J1545-4550	No	$9.1 \times 10^{33}$	0.18	$5.4 \times 10^5$	$1.2 \times 10^{12}$	2222	$2 \times 10^{10}$	11	$9.8 \times 10^{-15}$
J0024-7204Q	No	$4.1 \times 10^{33}$	0.21	$1.0 \times 10^5$	$4.1 \times 10^{11}$	4520	$2 \times 10^{10}$	12	$9.6 \times 10^{-15}$
J1811-2405	Yes	$5.8 \times 10^{33}$	0.27	$5.4 \times 10^5$	$1.3 \times 10^{12}$	1831	$2 \times 10^{10}$	16	$8.8 \times 10^{-15}$
J1653-2054	No	$1.3 \times 10^{33}$	0.091	$1.1 \times 10^5$	$4.1 \times 10^{11}$	2631	$2 \times 10^{10}$	5	$8.7 \times 10^{-15}$
J0557+1550	No	$3.5 \times 10^{33}$	0.23	$4.2 \times 10^5$	$1.0 \times 10^{12}$	1834	$2 \times 10^{10}$	14	$7.6 \times 10^{-15}$
J2022+2534	No	$2.6 \times 10^{33}$	0.077	$1.1 \times 10^5$	$4.2 \times 10^{11}$	4015	$2 \times 10^{10}$	5	$7.4 \times 10^{-15}$
J1906+0055	No	$1.2 \times 10^{33}$	0.13	$5.3 \times 10^4$	$2.6 \times 10^{11}$	4477	$2 \times 10^{10}$	8	$7.2 \times 10^{-15}$
J1142+0119	Yes	$9.1 \times 10^{32}$	0.18	$1.4 \times 10^5$	$4.9 \times 10^{11}$	2169	$2 \times 10^{10}$	11	$6.4 \times 10^{-15}$
J0509+0856	No	$5.2 \times 10^{32}$	0.13	$4.2 \times 10^5$	$1.0 \times 10^{12}$	817	$2 \times 10^{10}$	8	$5.8 \times 10^{-15}$
J1125-6014	Yes	$1.6 \times 10^{33}$	0.33	$7.6 \times 10^5$	$1.6 \times 10^{12}$	988	$2 \times 10^{10}$	20	$5.3 \times 10^{-15}$
J1903-7051	Yes	$1.8 \times 10^{33}$	0.34	$9.5 \times 10^5$	$1.8 \times 10^{12}$	930	$2 \times 10^{10}$	20	$4.8 \times 10^{-15}$
J2039-3616	Yes	$1.9 \times 10^{33}$	0.16	$5.0 \times 10^5$	$1.2 \times 10^{12}$	1705	$2 \times 10^{10}$	10	$3.8 \times 10^{-15}$
J1405-4656	No	$5.0 \times 10^{32}$	0.25	$7.7 \times 10^5$	$1.6 \times 10^{12}$	669	$2 \times 10^{10}$	15	$3.6 \times 10^{-15}$
J1630+3734	Yes	$2.3 \times 10^{33}$	0.27	$1.1 \times 10^6$	$2.0 \times 10^{12}$	1187	$2 \times 10^{10}$	16	$3.3 \times 10^{-15}$
J0614-3329	Yes	$4.4 \times 10^{33}$	0.32	$4.6 \times 10^6$	$5.3 \times 10^{12}$	630	$2 \times 10^{10}$	19	$3.2 \times 10^{-15}$
J2317+1439	Yes	$4.7 \times 10^{32}$	0.2	$2.1 \times 10^5$	$6.6 \times 10^{11}$	1667	$2 \times 10^{10}$	12	$3.1 \times 10^{-15}$
J1641+3627F	No	$4.1 \times 10^{33}$	0.16	$1.2 \times 10^5$	$4.5 \times 10^{11}$	7420	$2 \times 10^{10}$	9	$3.0 \times 10^{-15}$
J0925+6103	No	$6.0 \times 10^{32}$	0.15	$2.1 \times 10^5$	$6.5 \times 10^{11}$	1976	$2 \times 10^{10}$	9	$2.8 \times 10^{-15}$
J1741+1351	Yes	$4.5 \times 10^{33}$	0.28	$1.4 \times 10^6$	$2.4 \times 10^{12}$	1667	$2 \times 10^{10}$	17	$2.3 \times 10^{-15}$
J1216-6410	No	$2.9 \times 10^{32}$	0.18	$3.5 \times 10^5$	$9.2 \times 10^{11}$	1098	$2 \times 10^{10}$	11	$2.3 \times 10^{-15}$
J1017-7156	No	$1.4 \times 10^{33}$	0.22	$5.6 \times 10^5$	$1.3 \times 10^{12}$	1807	$2 \times 10^{10}$	13	$2.1 \times 10^{-15}$
J2129-5721	No	$3.2 \times 10^{33}$	0.15	$5.7 \times 10^5$	$1.3 \times 10^{12}$	3200	$2 \times 10^{10}$	9	$1.5 \times 10^{-15}$
J1804-2717	No	$4.0 \times 10^{32}$	0.23	$9.6 \times 10^5$	$1.8 \times 10^{12}$	805	$2 \times 10^{10}$	14	$1.5 \times 10^{-15}$
J1732-5049	Yes	$7.5 \times 10^{32}$	0.21	$4.5 \times 10^5$	$1.1 \times 10^{12}$	1874	$2 \times 10^{10}$	12	$1.4 \times 10^{-15}$
J1125+7819	No	$7.4 \times 10^{32}$	0.33	$1.3 \times 10^6$	$2.3 \times 10^{12}$	903	$2 \times 10^{10}$	20	$1.4 \times 10^{-15}$
J1857+0943	Yes	$9.1 \times 10^{32}$	0.28	$1.1 \times 10^6$	$2.0 \times 10^{12}$	1200	$2 \times 10^{10}$	17	$1.3 \times 10^{-15}$
J1921+1929	Yes	$1.6 \times 10^{34}$	0.3	$3.4 \times 10^6$	$4.3 \times 10^{12}$	2434	$2 \times 10^{10}$	18	$1.2 \times 10^{-15}$

Name	3PC	$L_{\text{MSP}}$	Mass	$P_{\text{orb}}$	Separation	Distance	Radius	Average Density	Peak Flux
Units	–	ergs/s	$M_{\odot}$	s	cm	pc	cm	$\text{g}/\text{cm}^3$	$\text{ph}/\text{cm}^2/\text{s}$
J2355+0051	No	$4.9 \times 10^{32}$	0.28	$1.0 \times 10^6$	$1.9 \times 10^{12}$	958	$2 \times 10^{10}$	17	$1.2 \times 10^{-15}$
J1921+0137	Yes	$9.8 \times 10^{33}$	0.27	$8.6 \times 10^5$	$1.7 \times 10^{12}$	5086	$2 \times 10^{10}$	16	$1.1 \times 10^{-15}$
J1125-5825	Yes	$1.6 \times 10^{34}$	0.31	$6.6 \times 10^6$	$6.7 \times 10^{12}$	1744	$2 \times 10^{10}$	18	$9.5 \times 10^{-16}$
J1858-2216	Yes	$2.2 \times 10^{33}$	0.25	$4.0 \times 10^6$	$4.7 \times 10^{12}$	921	$2 \times 10^{10}$	15	$9.4 \times 10^{-16}$
J1431-5740	No	$7.3 \times 10^{32}$	0.18	$2.4 \times 10^5$	$7.1 \times 10^{11}$	3553	$2 \times 10^{10}$	11	$9.3 \times 10^{-16}$
J1918-0642	No	$4.5 \times 10^{32}$	0.28	$9.4 \times 10^5$	$1.8 \times 10^{12}$	1111	$2 \times 10^{10}$	17	$9.0 \times 10^{-16}$
J1600-3053	Yes	$1.6 \times 10^{33}$	0.24	$1.2 \times 10^6$	$2.2 \times 10^{12}$	1887	$2 \times 10^{10}$	14	$7.8 \times 10^{-16}$
J2015+0756	No	$6.5 \times 10^{32}$	0.24	$5.6 \times 10^5$	$1.3 \times 10^{12}$	2086	$2 \times 10^{10}$	14	$7.4 \times 10^{-16}$
J0921-5202	No	$1.5 \times 10^{32}$	0.27	$3.3 \times 10^6$	$4.2 \times 10^{12}$	355	$2 \times 10^{10}$	16	$5.4 \times 10^{-16}$
J2042+0246	Yes	$1.2 \times 10^{33}$	0.22	$6.7 \times 10^6$	$6.6 \times 10^{12}$	640	$2 \times 10^{10}$	13	$5.3 \times 10^{-16}$
J1901+0300	No	$7.6 \times 10^{32}$	0.16	$2.1 \times 10^5$	$6.5 \times 10^{11}$	5304	$2 \times 10^{10}$	10	$5.2 \times 10^{-16}$
J1137+7528	Yes	$1.6 \times 10^{33}$	0.17	$6.2 \times 10^5$	$1.3 \times 10^{12}$	3833	$2 \times 10^{10}$	10	$4.9 \times 10^{-16}$
J1813-2621	No	$1.1 \times 10^{33}$	0.22	$7.1 \times 10^5$	$1.5 \times 10^{12}$	3158	$2 \times 10^{10}$	13	$4.2 \times 10^{-16}$
J1813-0402	No	$7.9 \times 10^{32}$	0.33	$9.1 \times 10^5$	$1.8 \times 10^{12}$	2229	$2 \times 10^{10}$	20	$4.0 \times 10^{-16}$
J1312+0051	Yes	$1.8 \times 10^{33}$	0.21	$3.3 \times 10^6$	$4.1 \times 10^{12}$	1471	$2 \times 10^{10}$	12	$3.9 \times 10^{-16}$
J1841+0130	No	$2.4 \times 10^{33}$	0.11	$9.0 \times 10^5$	$1.7 \times 10^{12}$	4230	$2 \times 10^{10}$	7	$3.7 \times 10^{-16}$
J0732+2314	No	$6.9 \times 10^{32}$	0.17	$2.6 \times 10^6$	$3.5 \times 10^{12}$	1151	$2 \times 10^{10}$	10	$3.4 \times 10^{-16}$
J1120-3618	No	$4.3 \times 10^{31}$	0.22	$4.9 \times 10^5$	$1.2 \times 10^{12}$	954	$2 \times 10^{10}$	13	$2.8 \times 10^{-16}$
J1929+0132	No	$2.6 \times 10^{32}$	0.31	$8.0 \times 10^5$	$1.6 \times 10^{12}$	1852	$2 \times 10^{10}$	19	$2.2 \times 10^{-16}$
J1643-1224	No	$1.5 \times 10^{33}$	0.14	$1.3 \times 10^7$	$1.0 \times 10^{13}$	740	$2 \times 10^{10}$	8	$2.2 \times 10^{-16}$
J1937+1658	No	$1.7 \times 10^{33}$	0.22	$1.5 \times 10^6$	$2.4 \times 10^{12}$	3259	$2 \times 10^{10}$	13	$2.1 \times 10^{-16}$
J2001+0701	No	$3.6 \times 10^{32}$	0.11	$4.5 \times 10^5$	$1.1 \times 10^{12}$	3782	$2 \times 10^{10}$	7	$1.7 \times 10^{-16}$
J1835-0114	No	$4.1 \times 10^{32}$	0.21	$5.8 \times 10^5$	$1.3 \times 10^{12}$	3457	$2 \times 10^{10}$	12	$1.7 \times 10^{-16}$
J1455-3330	Yes	$3.8 \times 10^{32}$	0.3	$6.6 \times 10^6$	$6.6 \times 10^{12}$	684	$2 \times 10^{10}$	18	$1.5 \times 10^{-16}$
J1751-2857	No	$1.5 \times 10^{33}$	0.23	$9.6 \times 10^6$	$8.4 \times 10^{12}$	1087	$2 \times 10^{10}$	13	$1.4 \times 10^{-16}$
J1828+0625	No	$7.8 \times 10^{32}$	0.32	$6.7 \times 10^6$	$6.8 \times 10^{12}$	1000	$2 \times 10^{10}$	19	$1.4 \times 10^{-16}$
J2019+2425	No	$9.1 \times 10^{32}$	0.36	$6.6 \times 10^6$	$6.7 \times 10^{12}$	1163	$2 \times 10^{10}$	22	$1.2 \times 10^{-16}$
J2236-5527	No	$2.3 \times 10^{32}$	0.26	$1.1 \times 10^6$	$2.0 \times 10^{12}$	2070	$2 \times 10^{10}$	16	$1.1 \times 10^{-16}$
J2302+4442	Yes	$7.8 \times 10^{32}$	0.34	$1.1 \times 10^7$	$9.4 \times 10^{12}$	863	$2 \times 10^{10}$	21	$9.6 \times 10^{-17}$
J1908+0128	No	$4.0 \times 10^{33}$	0.34	$7.3 \times 10^6$	$7.1 \times 10^{12}$	2627	$2 \times 10^{10}$	20	$9.1 \times 10^{-17}$
J1713+0747	Yes	$7.1 \times 10^{32}$	0.32	$5.9 \times 10^6$	$6.2 \times 10^{12}$	1316	$2 \times 10^{10}$	19	$8.6 \times 10^{-17}$
J0203-0150	No	$8.1 \times 10^{32}$	0.14	$4.3 \times 10^6$	$4.9 \times 10^{12}$	1837	$2 \times 10^{10}$	9	$8.1 \times 10^{-17}$
J1622-6617	No	$3.5 \times 10^{31}$	0.11	$1.4 \times 10^5$	$5.0 \times 10^{11}$	4045	$2 \times 10^{10}$	6	$7.0 \times 10^{-17}$
J1709+2313	No	$2.9 \times 10^{32}$	0.32	$2.0 \times 10^6$	$3.0 \times 10^{12}$	2179	$2 \times 10^{10}$	19	$5.5 \times 10^{-17}$
J1421-4409	No	$3.7 \times 10^{32}$	0.21	$2.7 \times 10^6$	$3.6 \times 10^{12}$	2085	$2 \times 10^{10}$	12	$5.4 \times 10^{-17}$
J1811-0624	No	$5.3 \times 10^{32}$	0.24	$8.1 \times 10^5$	$1.6 \times 10^{12}$	5801	$2 \times 10^{10}$	14	$4.8 \times 10^{-17}$
J2033+1734	No	$4.2 \times 10^{32}$	0.22	$4.9 \times 10^6$	$5.4 \times 10^{12}$	1740	$2 \times 10^{10}$	13	$3.9 \times 10^{-17}$
J1900+0308	No	$3.9 \times 10^{32}$	0.2	$1.1 \times 10^6$	$2.0 \times 10^{12}$	4801	$2 \times 10^{10}$	12	$3.6 \times 10^{-17}$
J1056-7117	No	$2.7 \times 10^{31}$	0.15	$7.9 \times 10^5$	$1.6 \times 10^{12}$	1689	$2 \times 10^{10}$	9	$3.1 \times 10^{-17}$
J1853+1303	No	$1.0 \times 10^{33}$	0.28	$1.0 \times 10^7$	$8.7 \times 10^{12}$	1887	$2 \times 10^{10}$	17	$3.0 \times 10^{-17}$
J1850+0124	No	$1.9 \times 10^{33}$	0.29	$7.3 \times 10^6$	$7.1 \times 10^{12}$	3385	$2 \times 10^{10}$	17	$2.6 \times 10^{-17}$
J1640+2224	Yes	$7.0 \times 10^{32}$	0.29	$1.5 \times 10^7$	$1.2 \times 10^{13}$	1370	$2 \times 10^{10}$	17	$2.2 \times 10^{-17}$
J1910+1256	No	$6.2 \times 10^{32}$	0.22	$5.1 \times 10^6$	$5.5 \times 10^{12}$	2778	$2 \times 10^{10}$	13	$2.1 \times 10^{-17}$
J1824-0621	Yes	$2.1 \times 10^{33}$	0.34	$8.7 \times 10^6$	$8.1 \times 10^{12}$	3534	$2 \times 10^{10}$	20	$2.1 \times 10^{-17}$
J2229+2643	No	$4.6 \times 10^{32}$	0.14	$8.0 \times 10^6$	$7.4 \times 10^{12}$	1800	$2 \times 10^{10}$	8	$2.1 \times 10^{-17}$
J1844+0115	No	$1.2 \times 10^{33}$	0.16	$4.4 \times 10^6$	$4.9 \times 10^{12}$	4358	$2 \times 10^{10}$	10	$2.0 \times 10^{-17}$
J1806+2819	No	$8.6 \times 10^{31}$	0.29	$3.8 \times 10^6$	$4.6 \times 10^{12}$	1330	$2 \times 10^{10}$	17	$1.9 \times 10^{-17}$
J1855-1436	Yes	$1.9 \times 10^{33}$	0.31	$5.3 \times 10^6$	$5.8 \times 10^{12}$	5127	$2 \times 10^{10}$	19	$1.7 \times 10^{-17}$
J1824+1014	Yes	$6.3 \times 10^{32}$	0.31	$7.1 \times 10^6$	$7.0 \times 10^{12}$	2904	$2 \times 10^{10}$	18	$1.2 \times 10^{-17}$
J1938+2012	No	$3.2 \times 10^{32}$	0.21	$1.4 \times 10^6$	$2.3 \times 10^{12}$	6301	$2 \times 10^{10}$	12	$1.2 \times 10^{-17}$
J1825-0319	No	$5.7 \times 10^{32}$	0.21	$4.5 \times 10^6$	$5.1 \times 10^{12}$	3862	$2 \times 10^{10}$	12	$1.2 \times 10^{-17}$
J2010+3051	No	$3.4 \times 10^{32}$	0.24	$2.0 \times 10^6$	$3.0 \times 10^{12}$	6450	$2 \times 10^{10}$	14	$7.4 \times 10^{-18}$
J1708-3506	No	$9.9 \times 10^{32}$	0.19	$1.3 \times 10^7$	$1.0 \times 10^{13}$	3320	$2 \times 10^{10}$	11	$6.9 \times 10^{-18}$
J1930+2441	No	$3.6 \times 10^{32}$	0.27	$6.6 \times 10^6$	$6.6 \times 10^{12}$	3267	$2 \times 10^{10}$	16	$6.1 \times 10^{-18}$
J1810-2005	No	$3.3 \times 10^{31}$	0.33	$1.3 \times 10^6$	$2.3 \times 10^{12}$	3513	$2 \times 10^{10}$	20	$4.2 \times 10^{-18}$
J1327-0755	Yes	$7.4 \times 10^{32}$	0.26	$7.3 \times 10^5$	$1.5 \times 10^{12}$	25000	$2 \times 10^{10}$	16	$4.1 \times 10^{-18}$

Name	3PC	$L_{\text{MSP}}$	Mass	$P_{\text{orb}}$	Separation	Distance	Radius	Average Density	Peak Flux
Units	–	ergs/s	$M_{\odot}$	s	cm	pc	cm	$\text{g}/\text{cm}^3$	$\text{ph}/\text{cm}^2/\text{s}$
J1913+0618	No	$6.0 \times 10^{32}$	0.33	$5.9 \times 10^6$	$6.2 \times 10^{12}$	5862	$2 \times 10^{10}$	20	$3.7 \times 10^{-18}$
J1955+2908	No	$1.0 \times 10^{33}$	0.21	$1.0 \times 10^7$	$8.7 \times 10^{12}$	6303	$2 \times 10^{10}$	12	$2.7 \times 10^{-18}$
J1529-3828	No	$3.5 \times 10^{32}$	0.19	$1.0 \times 10^7$	$8.8 \times 10^{12}$	4301	$2 \times 10^{10}$	11	$1.9 \times 10^{-18}$
J0407+1607	No	$3.7 \times 10^{31}$	0.22	$5.8 \times 10^7$	$2.8 \times 10^{13}$	1337	$2 \times 10^{10}$	13	$2.1 \times 10^{-19}$
J1912-0952	No	$1.4 \times 10^{31}$	0.085	$2.5 \times 10^6$	$3.4 \times 10^{12}$	9446	$2 \times 10^{10}$	5	$1.1 \times 10^{-19}$

TABLE S6: The line flux estimates for He WD-MSP systems in the ATNF Pulsar Catalogue. The values for companion mass and distance are taken from the ATNF Pulsar Catalogue [S80]. The companion mass used here is the median mass according to the ATNF Pulsar Catalogue. The separation is calculated from the orbit period listed in the ATNF Pulsar Catalogue. The radius is the lesser value of either the size of the Roche lobe or the radius of the model used in the Methods section. The density column is the average density assuming a homogeneous sphere with the companion mass and radius.